Scour around wind turbine foundations, marine pipelines and short cylinders due to long-crested and short-crested nonlinear random waves plus currents

Peder Hesten

May 31, 2011

Preface

This report represents my master thesis at Marin Teknikk, NTNU. It can be seen as a natural elongation of the pre-project I wrote last semester about wave run-up on circular slender piles in long-crested and short-crested nonlinear random waves as the wave theory is very much similar. The choice of research field is based on an personal interest in waves, stochastic theory of sealoads and the oportunity to make green energy alternatives more suitable for the marine environment.

The first periode of this semester involved gathering background information and getting updated on the reseach which forms the baseline. Secondly, I implemented the method in Matlab and generated the results. Finally, I discussed the results and wrote the report. The main challenges have been to get understanding of all the aspects of this method as it turned out to be more complex than first expected. Also, comprehending the mechanisms of short-crested and long-crested waves has been a challenge. Personally, this have been a rewarding and informative process. My supervisors, Professor Dag Myrhaug and Post-doc Muk Chen Ong have been avaliable troughout the whole semester for motivating discussions and guidance and for that I am very grateful.

Peder Hesten

Contents

List of Figures

List of Tables

Summary

This report presents a stochastic method for predicting scour depth around vertical circular slender piles, including various cross sections and group arrangements, marine pipelines and the burial and scour hole geometry around short cylinders due to long-crested (3D) and short-crested (2D) nonlinear random waves plus current. The waves are assumed to be stationary narrowbanded and the Forristall (2000) distribution of wave crest heights representing 2D and 3D random waves is employed including both sum-frequency and difference-frequency effects. The wave crests are assumed to be responsible for the scour response. The results for scour and burial around the various structure types are presented graphically versus a measure of the wave action evaluated at the seabed relative to the characteristic diameter of the structure and versus a measure of the current velocity relative to the maximum horizontal fluid particle velocity at the seabed. The ratios between the scour depth predicted by 3D, 2D and linear waves are also investigated. Examples of calculation based on typical field conditions are provided. Due to the distinctive character of the Forristall distribution, all the results are specifically given by the seastate and the characteristic structure diameter. There are several similarities in the ratios of the scour depth for the various structures. Overall, 3D and 2D waves will produce more scour and burial than linear waves. This is due to higher fluid particla velocity under the wave crests for 3D and 2D waves compared to linear waves. In deep water, the scour depth from 2D waves is largest and in finite water depth the scour depth from 3D waves is largest. This is due to larger sum-frequency effects for 2D waves compared to 3D waves in deep water and smaller difference-frequency effects for 3D waves compared to 2D waves in finite water depth.

1 Introduction

Scour is erosion of seabed sediments around a structure due to flow velocities induced by waves or current, Sumer and Fredsøe (2002). A vertical pile or a horizontal pipeline installed on the seabed are subjects to the boundary layer of the flow. In deep water, this flow is likely to be a steady current, whereas in finite water depth the orbital motion from the waves will propagate down to the seabed leading to combined waves and current situations. The structures may also be subject to waves alone. The typical design conditions for structures situated in the North Sea is wave dominated flow with seabed consisting of fine sand. The complicated flow situation caused by the presence of the structure, the seabed and the incoming flow can cause scour holes around the structure. For a pile this means that even though it was mounted on a flat seabed, it may after some time be surrounded by a scour hole which may lead to a decrease in stability. A pipeline carrying oil or gas which initially is resting on a flat seabed may suffer from free spans or be partially buried during the lifetime. If the free span is large the risk of experiencing vibrations due to the incoming flow will increase. Sea mines, or short cylinders, placed on the seabed may be surrounded by scour holes and buried. Overall, the resulting scour response depends on the geometry of the seabed, the seabed material, the velocity of the incoming flow and ratio between the orbital fluid particle displacement and the characteristic dimension of the structure. Further, real life wave crests are nonlinear and may display a complex three-dimensional random pattern which makes the situation more complicated.

For regular waves, Sumer and Fredsøe (1990) proposed empirical formulas for the scour depth around pipelines. The corresponding formulas for vertical piles were presented in Sumer et al. (1992). By utilizing these formulas and describing the waves as a stationary Gaussian narrowband process Myrhaug and Rue (2003) presented a method for calculating the scour depth around pipelines and vertical piles in random waves. For the case of vertical piles, the influence of cross sectional shape in regular waves was investigated trough laboratory experiments by Sumer et al. (1993) and they stated that their original formula from Sumer et al. (1992) was applicable provided that the coefficients were given new values based on best fit to the data. Further, Sumer and Fredsøe (1998) investigated the influence on scour depth for various group arrangements of piles in regular waves trough experiments. Based on that, Myrhaug and Rue (2003) found new coefficients to be employed in the original formula from Sumer et al. (1992).

For irregular waves plus current, Sumer and Fredsøe (1996) presented results of and experimental study and proposed empirical formulas for the scour depth around pipelines. The corresponding formulas for vertical piles were presented in Sumer and Fredsøe (2002) based on experimental data from Sumer and Fredsøe (2001). Myrhaug et al. (2009) employed these formulas to find the scour depth around pipelines and vertical piles due to second-order random waves plus current. They assumed that the wave motion was a stationary Gaussian narrowbanded process and compared their model to the experimental data from Sumer and Fredsøe (1996, 2001) for pipelines and piles, respectivly.

Catano-Lopera and Garcia (2006, 2007) studied the burial and scour hole geometry around a short cylinder resting on the seabed subject to regular waves plus current. By employing these formulas and assuming the wave motion to be a stationary Gaussian narrowbanded pro-

cess Myrhaug and Ong (2009) presented a stochastic model for random waves and currents including effects of second order wave asymmetry.

The purpose of this report is to provide a method for calculating scour depth around pipelines, vertical piles and the burial and scour hole geometry around short cylinders caused by short-crested (2D) and long-crested (3D) nonlinear random waves plus current. The wave motion is assumed to be a stationary narrowband random process and the Forristall (2000) distribution of wave crests is employed to describe both 2D and 3D random waves. The empirical formulas for scour depth in irregular waves plus current shall be employed

2 Background

The pressurefield around the structure will change due to the presence of the strucure. In general there will be an increase in the bed shear stress and in the level of turbulence compared to areas where the flow is unaffected by the structure. As a consequence of this the sediment transport rate is higher in the neighbourhood of the structure compared to areas far away where the structure has no impact on the flow. Scour is defined as erosion of the sediments on the seabed related to the presence of a structure, Sumer and Fredsøe (2002). The amplification in the bed shear stress can be described by the amplification factor defined as

$$\alpha = \frac{\tau}{\tau_\infty} \tag{1}$$

where τ is the bed shear stress around the structure and τ_∞ is the bed shear stress far away from the structure in the undistrubed flow. The scour prosess will continue until the scour hole reaches a depth where $\tau \approx \tau_\infty$. This is called the equilibrium scour depth. At this condition the sediments may still move around but the depth of the hole does not change. The time it takes for this amount of scour to develop is called the time scale of the process. The following definition is taken from Sumer et al. (1992):

$$S_t = S(1 - \exp{(-\frac{t}{T})}) \tag{2}$$

where T is the time scale of the scour, S is the equilibrium scour depth and S_t is the instantanious scour depth at the time t. Fig. 1 illustrates a typical development of scour depth. It appears that after a certain amount of time the depth of the scour hole remains constant. Both the equilibrium scour depth and the timescale is of great importance for engineering purposes. The greatest scourdepths often takes place during storms and it is essential to assess whether the storm lasts longer than the neccesary timescale of the scour.

2.1 Shields parameter in regular waves

Scour can be devided in two types; clear-water scour and live-bed scour. The class is determined by the Shields parameter, θ, given as, Sumer and Fredsøe (2002)

$$\theta = \frac{\tau_\infty}{\rho g(s-1)d_{50}} \tag{3}$$

where s is the ratio between the sediment density, ρ_s, and the fluid density, ρ. d_{50} is the median grain diameter and g is the acceleration of gravity. θ_{cr} is the critical value of the

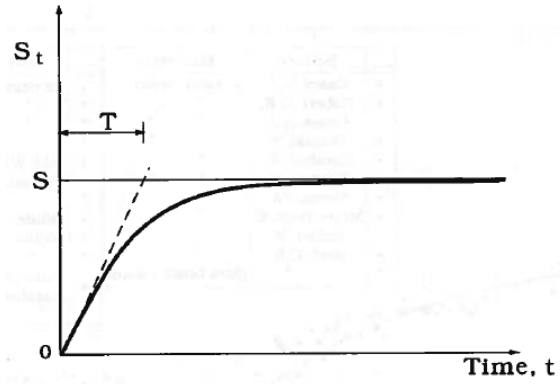

Figure 1: Typical development of scour with time, taken from Sumer and Fredsøe (2002).

Shields parameter. Sumer and Fredsøe (2002) states that for $\theta < \theta_{cr}$ the shear force is not large enough to initiate any sediment motion on the seabed far from the structure. This class is named clear-water scour. When $\theta \geq \theta_{cr}$ the class of live-bed scour is reached and the sediments will be transported over the entire seabed. For any changes in θ larger than the critical value there will be a corresponding change in the motion of the sediments. It should be noticed that the same formula can utilized to assess the Shields parameter in the neighbourhood of the structure by using τ instead of τ_∞. If a structure is placed on a seabed where $\theta < \theta_{cr}$ initially, live-bed scour might still occur in the neighbourhood of the structure if the resulting change in shear stress caused by the structure is sufficiently large. It is common to assume that $\theta_{cr} \approx 0.05$.

The maximum bottom shear stress under the waves far away from the structure is given as

$$\tau_\infty = \frac{1}{2} f_w U_m^2 \tag{4}$$

where U_m is the maximum horizontal fluid particle velocity evaluated at the seabed and f_w is a friction factor given in Myrhaug et al. (2001) as

$$f_w = c(\frac{A}{z_0})^{-d} \tag{5}$$

where z_0 is the seabed roughness given as $d_{50}/12$ and A is the amplitude of the orbital displacement of the water particles near the seabed related to the linear wave height H as

$$A = \frac{H}{2 \sinh kh} \tag{6}$$

h is the water depth and k is the wave number given by the dispersion relationship

$$\omega^2 = kg \tanh kh \tag{7}$$

f_w can be applied for waves plus current in seastates dominated by waves. The coefficients c and d are based on best fit to data and given as

$$(c, d) = (18, 1) \quad \text{for} \quad 20 \lesssim A/z_0 \lesssim 200 \tag{8}$$

$$(c, d) = (1.39, 0.52) \quad \text{for} \quad 200 \lesssim A/z_0 \lesssim 11000 \tag{9}$$

$$(c, d) = (0.112, 0.25) \quad \text{for} \quad 11000 \lesssim A/z_0 \tag{10}$$

By utilizing this model to assess the bed shear stress it is possible to find an analytical expression for the Shields parameter in random waves. More details on this will be given in Section 6.4

3 Scour around a vertical slender pile

3.1 Mechanisms

Scour around a vertical slender pile placed on the seabed is caused by two main mechanisms, the horseshoe vortices in front and the lee-wake vortices at the downstream side of the pile. The rotation, caused by the seabed boundary layer, in the incoming flow causes a downstream as the flow interacts with the adverse pressure gradient caused by the presence of the pile. Fig. 2 is a definition sketch of a pile in a flow. At the intersection between the pile and the seabed the flow rotates away from surface of the pile, creating the horseshoe vortices which is carried by the flow around the pile. Fig. 3 illustrates a profile of the velocity vector diagram at $y = 0$ upstream of the pile. The lee-wake vortices are caused by the separation of the boundary layer on the surface of the pile. In terms of scour, the most important mechanism is the horseshoe vortices.

For a pile standing in a steady current the size of the horseshoe vortices depends on the ratio between the seabed boundary layer thickness the geometry and diameter of the pile and the pile-based Reynolds number given as $R_{e_D} = U_m D/\nu$ where D is the pile diameter and ν is the kinematic viscosity of the water. According to Sumer and Fredsøe (2002), if the ratio between the boundary layer thickness and the pile diameter is high, the room for horseshoe vortices will increase. A small Reynolds number involves high viscosity and the seabed boundary layer must overcome more resistance in order to seperate.

For a pile situated in waves, the Keulegan-Capenter number, KC, must also be considered. It is given as

$$KC = \frac{U_m T}{D} \tag{11}$$

where T is the wave periode. Moreover, $U_m = A\omega$ where $\omega = 2\pi/T$ is the angular wave frequency. By utilizing this the Keulegan-Carpenter number can be rewritten as

$$KC = \frac{2\pi A}{D} \tag{12}$$

It now appears that KC is proportional to the ratio between the orbital displacement of the water particles, $2A$, and the diameter of the pile. For small values of KC the movement of the water particles is small compared to the diameter of the pile and the horseshoe vortices may not have time to form. For very large values of KC, e.g. a tidal current, the flow can be regarded as a steady current within each half periode.

Sarpkaya (1986) states that the boundary layer flow on a cylinder surface will be laminar for $KC \leq 1$. Fig. 4 shows the results of an experimental study by Sumer et al. (1997) of

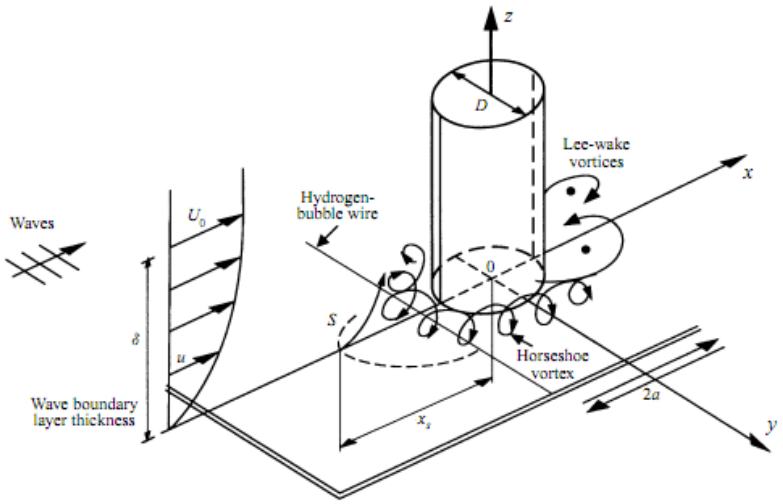

Figure 2: Principal sketch of boundary layer flow interacting with vertical pile, taken from Sumer et al. (1997).

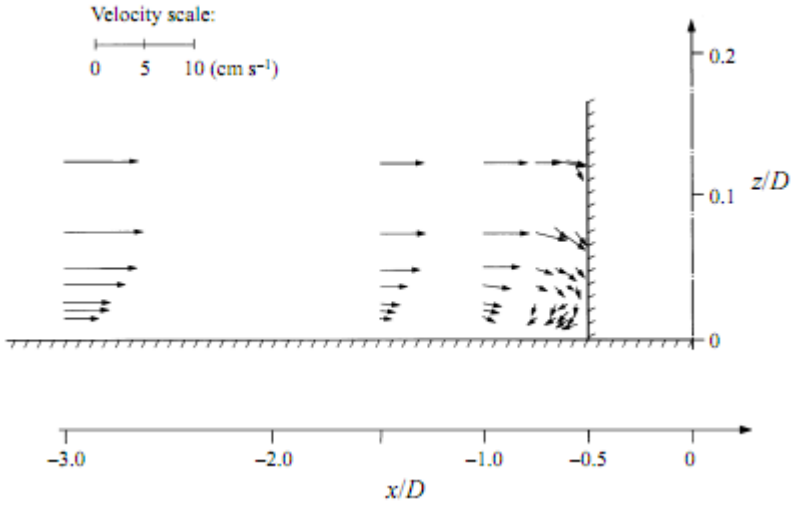

Figure 3: Formation of horseshoe vortices illustrated by vectors for $KC = 10.3$ and $\omega t = 90$ deg, taken from Sumer et al. (1997).

horseshoe vortices in waves for different KC numbers and Reynolds number of $O(3)$. For simplicity it is now assumed that the orbital horizontal fluid velocity at the seabed, U, can be written as $U = U_m \sin \omega t$. When $\omega t = 0°$ the velocity at the seabed is zero and obviously there is no formation of horseshoe vortices for any KC-number. For $90° \leq \omega t \leq 150°$ it appears that the horseshoe vortices will form at the front of the pile for KC-numbers larger than about 6. The formation of horseshoe vortices at the back of the pile is more limited in terms of ωt but the lowest KC-number is still 6. The reason for the asymmetric behaviour in the graphs is due to nonlinearity in the waves. It appears that for increasing KC-number the horseshoe vortices occurs for a larger part of the wave phase, both in front and back of the pile. The flow will separate along the surface of the cylinder for $KC > 1$ but the horseshoe vortices do not occur until $KC = 6$. The reason for this is related to the different adverse pressure gradients. Sumer and Fredsøe (2002) presents expressions for the pressure gradient along side surface and in front of the pile. It appears that the maximum value of the pressure gradient along the pile surface is about 5 times larger than the pressure gradient in front of the pile, causing separation for smaller orbital displacements of the water particles. The result of that difference is that the flow in front of the pile separates at $KC = 6$ and the flow at the surface of the pile separates for $KC = 1$.

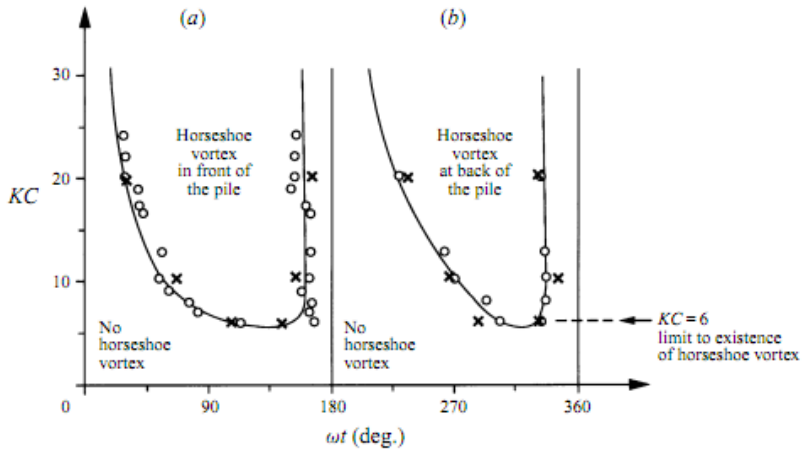

Figure 4: Formation of horseshoe vortices as function of KC-number and wave phase, o marks flow visualization experiments, + marks measurements of bed shear stress, Sumer et al. (1997).

Fig. 5 shows isocurves for α for $KC = 6.1$ and current alone. The waves propagate along the positive x-axis. It appears that the largest values of α are found at the sides of the pile. In addition to the horseshoe vortices, this location gets a large contribution from contraction of streamlines. For the current alone case, the maximum $\alpha \approx 10$ suggesting a strong contribution from horse shoe vortices. The corresponding value for $KC = 6.1$ is about 4.5.

3.2 Regular waves

Fig. 6 shows the definition of scour depth for a vertical pile with diameter D. From the previous discussion it is clear that, within certain limits, an increase KC will lead to a deeper scour hole. The horseshoe vortices grows stronger and the half period of the orbital wave

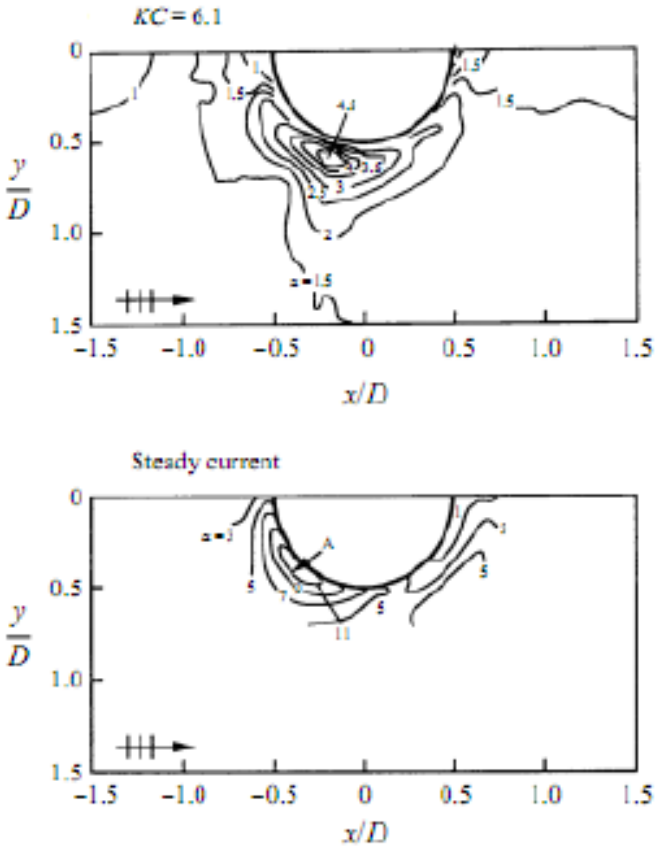

Figure 5: Isocurves for α , Sumer et al. (1997).

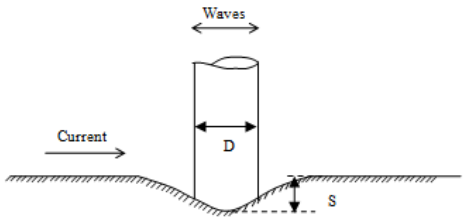

Figure 6: Definition of scour depth around vertical pile, taken from Myrhaug et al. (2009).

motion grows longer, allowing the vortices more time to grow strong, Sumer and Fredsøe (2002). Through a series laboratory experiments Sumer et al. (1992) obtained the following empirical formula for the equilibrium scour depth in regular waves for live-bed conditions provided that the timescale of the scour has been exceeded.

$$\frac{S}{D} = C(1 - \exp\left[-q(KC - r)\right]) \quad \text{for} \quad KC \geq r \tag{13}$$

C, q and r are dimensionless coefficients given by the following values for the case of waves alone

$$(C, q, r) = (1.3, 0.03, 6) \tag{14}$$

$r = 6$ appears to be consistent with the previous discussion. It should be noted that for $KC \to \infty$, S/D will approach $C = 1.3$.

3.3 Pile with square cross section

Sumer et al. (1993) presented results of an experimental study on the influence of cross-sectional shape on scour depth in regular waves with slender vertical piles. Fig. 7 is based on their experimental data and illustrates S/D versus KC for circular, 90° square and 45° square pile. It appears that the effect of cross section is largest for the lower values of KC. Starting from $KC = 0$ the onset of scour occurs first for the 45° square pile, followed by the circular and the 90° square pile. As a consequence, the 45° square pile will experience the largest scour depth. This is related to the dominating vortex shedding at low values of KC.

For high $KC \gtrsim 100$, the differences are small. This is due to low influence by the vortex shedding as the wave motion can be regarded as a steady current.

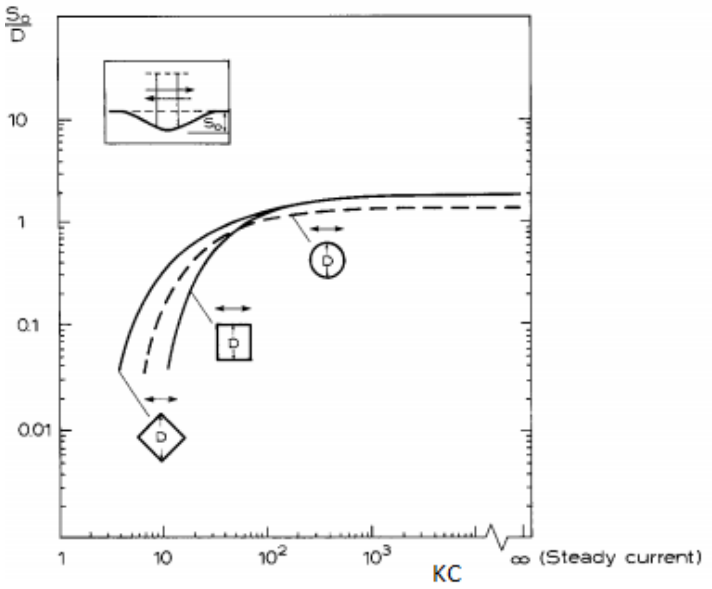

Figure 7: Equilibrium scour depth for various cross sections, Sumer et al. (1993).

Sumer et al. (1993) found that the empirical formula in Eq. (13) can still be employed but with the following values for the coefficients C, q and r

- 90° orientation:

$$(C, q, r) = (2, 0.015, 11) \tag{15}$$

- 45° orientation:

$$(C, q, r) = (2, 0.019, 3) \tag{16}$$

It should be noted that the current is not accounted for in this case.

3.4 Group of slender piles

3.4.1 Effect of pile spacing

The supporting structure of marine platforms are often made up of several piles grouped together. If the gap between the piles, G, is small compared to the diameter of the piles the interference effects will cause changes in the equilibrium scour depth compared to the case of the single pile alone, Sumer and Fredsøe (2002). Sumer and Fredsøe (1998) presented experimental data of scour around groups of vertical piles in regular waves. Fig. 8 illustrates the two pile arrangements that they investigated. As mentioned, the horseshoe vortex is the

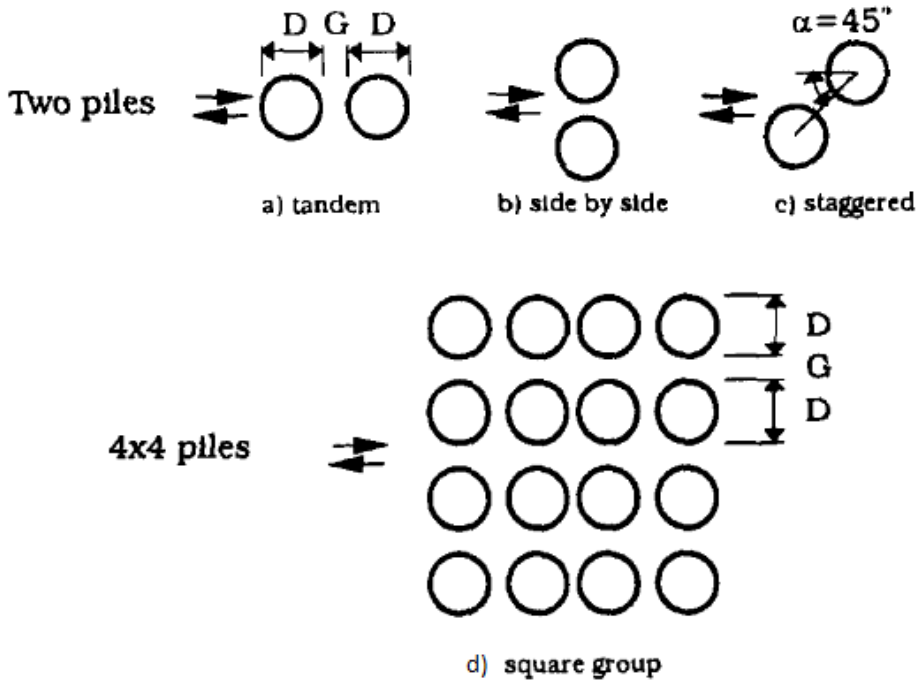

Figure 8: Various group arrangements of piles, taken from Sumer and Fredsøe (1998)

govurning mechanism for single pile scour, but for the case of groups of piles, especially tandem organized, the lee-wake vortices are also of great importance. If the piles are sufficiently close, the lee-wake vortices created by the upstream pile will influence the flow behaviour around the downstream pile, resulting in a change in scour depth. On the other hand, if the gap between the piles is very large the scour depth around each pile will not be influenced by the presence of the other pile and may therefore be treated as a single pile case. From Eq. (13) it appears that the single pile scour depth for live-bed contitions is a function of the

Keulegan-Carpenter number. For the case of pile groups the non-dimensional pile spacing G/D will also influence the result, implying that the non-dimensional scour depth can be written as

$$\frac{S}{D} = f(KC, \frac{G}{D}) \tag{17}$$

The results from Sumer and Fredsøe (1998) are illustrated in Fig. 9. Here the equilibrium scour depth for each of the two pile arrangements in Fig. 8 are illustrated as a function of the non-dimensional pile spacing for live-bed conditions with $KC = 13$.

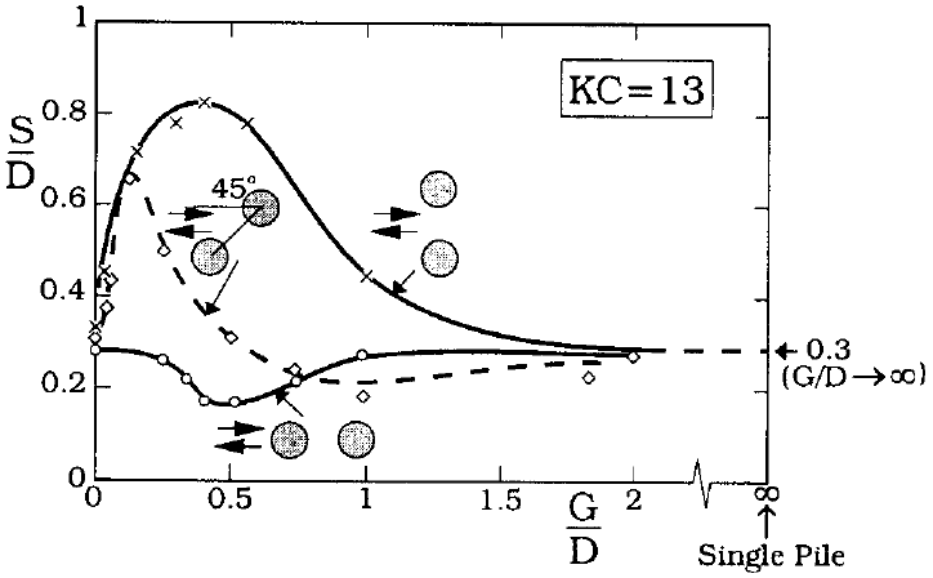

Figure 9: Equilibrium scour depth as function of G/D for two-pile arrangements, taken from Sumer and Fredsøe (1998)

For the side-by-side arrangement, Sumer and Fredsøe (1998) found that the maximum scour depth was located in the middle of the two piles for $0.1 < G/D < 2$. When the gap is small ($G/D < 0.1$) the pile pair will act as a single pile and the maximum scour depth is found at the outside edges of the piles. For $G/D > 2$, all interference effects between the piles fade out and each pile can be treated as a single pile standing alone. This is illustrated in Fig. 9. Moreover, it appears that the non-dimensional scour depth reaches a maximum value of about 0.83 at $G/D \approx 0.4$. For larger gaps it decreases to the single pile value. So, for decreasing G/D in the interval $(0.4, 2)$ there is an increase in the scour depth. This is partly due to an increase in the sediment transport rate in the gap flow and partly to the stronger presence of lee-wake vortices on the outer sides of the pile, Sumer and Fredsøe (2002).
The behaviour for the tandem arrangement is quite opposite of the side-by-side case. For G/D in the approximate range of 0.2 to 1 there is a dip in the maximum scour depth which is due to supression of the vortices shed by the upstream pile. If $G/D \lesssim 0.2$ the two piles may be treated as a single pile and the vortex shedding is re-established. Accordingly, the maximum scour depth will be equal to the case of the single pile. For $G/D > 1$ the interference effects may be neglected and the piles may be regarded as two independent single piles.
The behaviour of the 45° staggered arrangement is similar to the side-by-side case except that

the maximum scour depth is lower and occurs at lower G/D. This is caused by decreased impact from the gap-flow effect as described in Sumer and Fredsøe (2002).

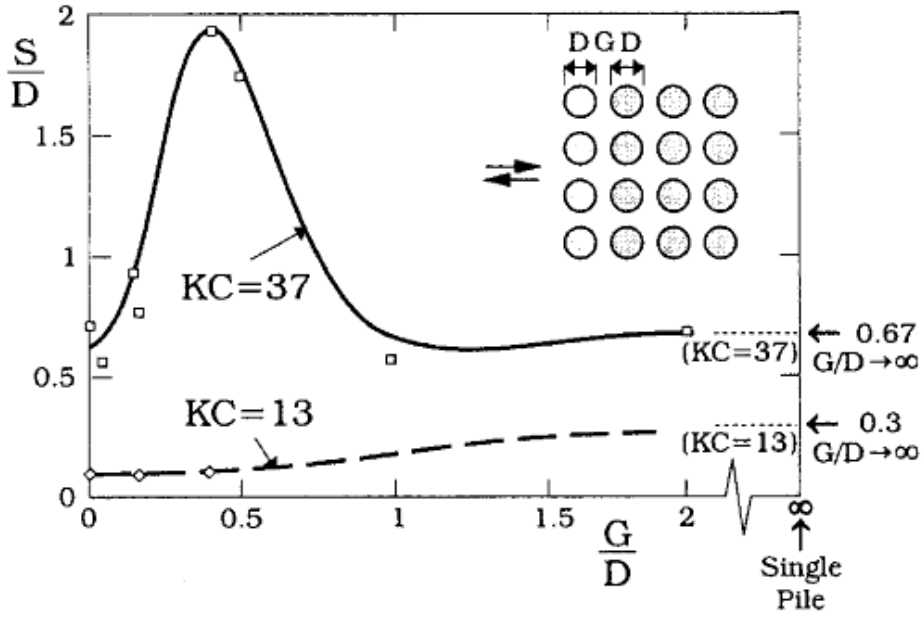

Figure 10: Equilibrium scour depth as function of G/D for square pile group, Sumer and Fredsøe (1998)

Fig. 10 illustrates the maximum equilibrium non-dimensional scour depth as a function of pile spacing for a 4×4 square pile group arrangement for two KC-numbers, $KC = 37$ and 13. According to Sumer and Fredsøe (1998), the maximum scour depth is always located around the corner piles in the first row. For $G/D > 2$ it appears that the non-dimensional scour depth approaches the same value as all the two-pile arrangements for the same KC-number, $KC = 13$. Moreover, when the gap is zero it is assumed that the group of piles is transformed into a large 90° square pile with a diameter $4D$. In order to account for this the square single piles will have a KC-number of $KC = 37/4 = 9.3$. For the square cross section pile in Fig. 7 this value of KC corresponds to $S/4D \approx 0.1$ or $S/D \approx 0.4$. From Fig. 10 it appears that the corresponding value is 0.6 which is not very different from 0.4. The difference may be explained by the sharp edges on the solid pile in Fig. 7, the rough, bumpy surface of the present single body and the possible presence of steady streaming. The latter is caused by disturbances in the flow caused by large piles, more on details on this subject can be found in Chapter 6.3 in Sumer and Fredsøe (2002).

3.4.2 Effect of KC-number

Fig. 11 shows the influence of the KC-number on the non-dimensional scour depth for the single slender pile, the 4×4 square pile group, the two-pile side-by-side arrangement and the two-pile 45° staggered arrangement for a constant pile spacing of $G/D = 0.4$. Firstly, it appears that the onset of scour for the two-pile groups occurs for lower KC than the case of the single pile. According to Sumer and Fredsøe (1998), this is related to the presence of

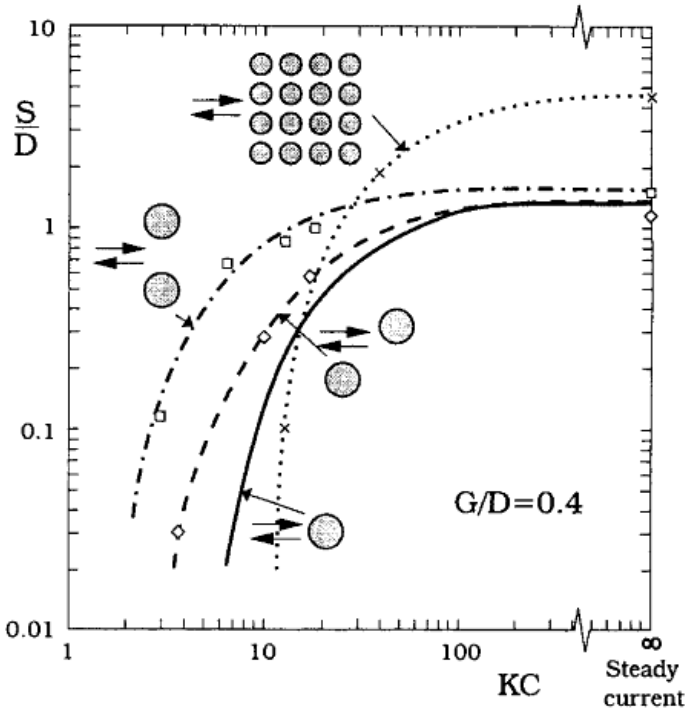

Figure 11: Equilibrium scour depth as function of KC for square pile group, Sumer and Fredsøe (1998)

gap flow at low KC-numbers for two-pile groups. Furthermore, for the lowest values of KC the scour depth around the two-pile arrangements is much larger compared to the single pile case. For $KC = 7$ the scour response around the side-by-side arrangement is magnified by a factor of about 25 compared to the single pile case. This is mainly caused by gap-flow effects. The onset of scour for the 4×4 square pile arrangement occurs at $KC \approx 12$ which is about twice the value compared to that of the single pile case. This is verified in Fig. 10 as the scour response for $KC = 13$ is much lower compared to the case for $KC = 37$ and caused by a weak gap flow for low values of KC. However, for increasing KC the horseshoe vortices becomes more dominant and the scour respons becomes more violent compared the other arrangements. When $KC \approx 300$ the difference in scour depth is about a factor of $3 - 4$ compared to the single pile case.
Overall, it appears from Fig. 11 that the scour around the groups is basically dominated by the same mechanisms as the single pile. For low KC numbers the lee-wake vortices are the governing flow processes but the horseshoe vortices are dominant when KC is increased.
Based on the data presented in Fig 11 and Table 4 in Sumer and Fredsøe (1998), Myrhaug and Rue (2005) found that Eq. (13) can be employed to calculate the maximum equilibrium scour depth around groups of vertical piles provided that the coefficients (C, q, r) are given by the following values

- Two-pile side-by-side arrangement:

$$(C, q, r) = (1.5, 0.09, 2) \tag{18}$$

- Two-pile 45° staggered arrangement:

$$(C, q, r) = (1.3, 0.037, 3) \tag{19}$$

- 4×4 square pile arrangement:

$$(C, q, r) = (4.5, 0.023, 12) \tag{20}$$

3.5 Waves plus current

Sumer and Fredsøe (2001) performed experiments with a single vertical pile standing in irregular waves plus current with KC ranging from 5 to 26. By trial and error they concluded that their formula for equilibium scour depth in Eq. (13) can be employed for irregular waves if KC is calculated as $KC_{SF} = U_{rms}T_p/D$, where T_p is the peak periode of the wave spectrum and U_{rms} is the root-mean-square, rms, value of U_m. Based on these data Sumer and Fredsøe (2002) porposed a model for calculating the equilibrium scour depth around a vertical pile in irregular waves plus current. Eq. (13) is still employed but the effect of current is accounted for in the coefficients q and r as follows

$$q = 0.03 + 0.75U_{cwrms}^{2.6} \tag{21}$$

$$r = 6\exp(-4.7U_{cwrms}) \tag{22}$$

where the dimensionless quantity U_{cwrms} is given as

$$U_{cwrms} = \frac{U_c}{U_c + U_{rms}} \tag{23}$$

U_c is the undisturbed current velocity. It should be noted that if the current velocity is zero then r and q will take the values given in Eq. (14). Further Eqs. (21) and(22) are given for wave dominated seastates, meaning $0 \leq U_{cwrms} \leq 0.4$. For waves plus current the dispersion relationship becomes $\omega = kU_c + (kg\tanh kh)^{1/2}$ which can be employed to determine k if U_c, ω and h are given. However, for wave dominated situations it is assumed that U_c can be neglected as the influence of U_c on k_p is small. C is independent of the presence of current. By inspection of the experimental data from Sumer and Fredsøe (2001), it was found by e.g. Myrhaug and Rue (2003) that T_p, used in KC_{SF}, is larger than the mean zero-crossing wave periode T_z. More accurately, $T_p = 1.5T_z$ which indicates that the spectrum used for the experiments was not narrowbanded. If the rms value of KC is given as

$$KC_{rms} = \frac{U_{rms}T_z}{D} \tag{24}$$

it follows that

$$KC_{SF} = 1.5KC_{rms} \tag{25}$$

For the case of regular waves plus current it is now assumed that Eqs. (13), (21) and (22) can be employed to calculate the maximum equilibrium scour depth around a circular slender pile provided that U_{rms} and KC_{SF} are substituted with U_m and KC respectivly. In r and q in Eqs. (21) and (22) the current is now accounted for by replacing U_{cwrms} with U_{cw} given as

$$U_{cw} = \frac{U_c}{U_c + U_m} \tag{26}$$

This procedyre has been employed by Myrhaug and Rue (2005) among others. It should be noted that the relation $T_p = 1.5T_z$ is only valid when discussing the experimental data by Sumer and Fredsøe (2001). This is also valid for the case of scour around a pipeline. Further, for the single piles with square cross-sections and the group arrangements of piles the current velocity is not accounted for.

4 Scour around a pipeline

4.1 Mechanisms

Marine pipelines are placed on the seabed to provide transportation of gas and oil from the offshore platforms. They can also serve other purposes like carrying waste from the platforms. The length of the pipes may be from hundreds to thousands of meters and the diameter can vary from 20-30 cm to over 1 m. In several ways, the pipelines acts as the blood veins of the oil and gas industry. Over the last 30 years tens of thousands of kilometers of pipeline have been installed on the seabed in oil fields across the world, Myrhaug et al. (2009).

4.1.1 Stages of scour

The scour prosess around a pipeline may be devided into four stages; Onset of scour, tunnel erosion, lee-wake erosion and the equilibrium stage. The presence of the pipeline causes a pressure difference between the upstream and downstream side of a pipe exposed to a current. The onset of scour occurs if the pressure difference is sufficiently large to induce a seepage flow underneath the pipeline in the sand, Sumer and Fredsøe (2002). A critical point is reached when the current velocity is increased further and the seepage flow develops faster than the driving pressure difference calls for, causing the bed surface on the downstream of the pipeline to rise. Eventually a mixture of sand and water breaks through underneath the pipeline. This phenomenom is called piping, Sumer and Fredsøe (2002). In a steady current the sand is constantly exposed to the pressure gradient. In waves, the pressure gradient produced in the half wave periode characterized by the trough is not large enough to generate piping and only the half periode characterized by the crest will contribute to piping, Sumer and Fredsøe (2002).

The next stage is tunnel erosion and is characterized by a small gap underneath the pipeline, see Fig. 12. A large amount of water is directed through this gap, likely causing high velocities and large shear stresses on the bed below the pipe. Jensen et al. (1990) performed experiments with a pipeline in a steady current and measured the amplification factor α in the gap. They found that α was in the range of 3 to 5 dependent on the current speed. According to Sumer and Fredsøe (2002) a enhancement factor of 4 in α will result in a factor of 8 increase in the sediment transport rate, suggesting a violent flow of a mixture of water and sand underneath the pipeline. The result can be formation of dunes on the downstream side of the pipe. As the gap grows larger the flow velocity will start to decrease which represents the closure of tunnel erosion and the beginnning of the stage called lee-wake erosion. Vortex shedding will begin to occur and the dunes will migrate further downstream.

The vortices that are shed from the downwards side of the pipeline sweep the downstream seabed causing an increase in the seabed shear stress.

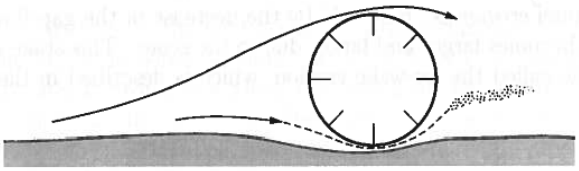

Figure 12: Tunnel erosion below pipeline, Sumer and Fredsøe (2002).

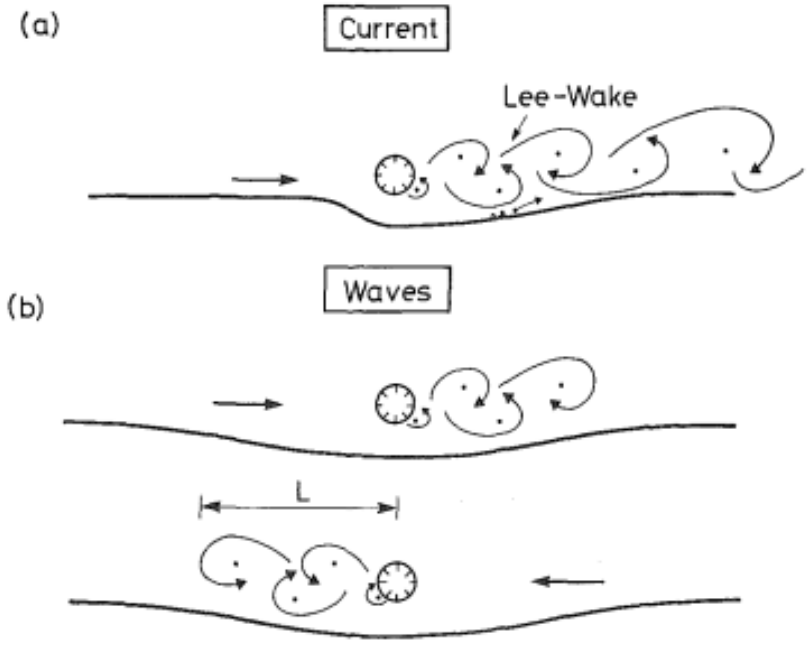

Figure 13: Lee-wake vortices in steady current (a) and waves (b), Sumer and Fredsøe (1990).

Fig. 13 shows the lee-wake vortices for the case of a steady current and waves. It appears that the slope of the upstream scour hole for the steady current is much larger compared to the downstream side. This is due to the lee-wake vortex erosion. For the case of waves, the scour hole is symmetric due to the orbital motion of the water particles. The equilibrium stage in the scour process is reached when the scour depth is steady. Now the Shields parameter in the hole is equal to the undisturbed Shields parameter meaning that the sediment transport rate is constant over the bed. The amount of sediments that comes into the hole is also carried out in this stage.

4.2 Regular waves

The vortex shedding mechanism is governed by the Keulegan-Carpenter number, KC, in wave dominated seastates, Sumer and Fredsøe (2002). For small values of KC the vortex shedding may not occur. On the other hand, for large values of KC the lee-wake vortices travels over a larger part of the seabed contributing to the sediment transport. The flow will in this case

erode more on the side of the scour hole making the slopes less steep. The area below the pipe will now be less protected against the outer flow, leading to higher velocities and more sediment transport, Sumer and Fredsøe (2002). If $KC \to \infty$ it can be assumed that the flow in each half periode will behave like a steady current.

For a pipeline with diameter D subject to regular waves the equilibium scour depth, S, is found based on experimental data from Sumer and Fredsøe (1990) as

$$\frac{S}{D} = 0.1\sqrt{KC} \tag{27}$$

for live-bed conditions. The equilibrium scour depth S is defined in Fig. 14. Eq. (27) is based on data in for $2 \geq KC \geq 1000$.

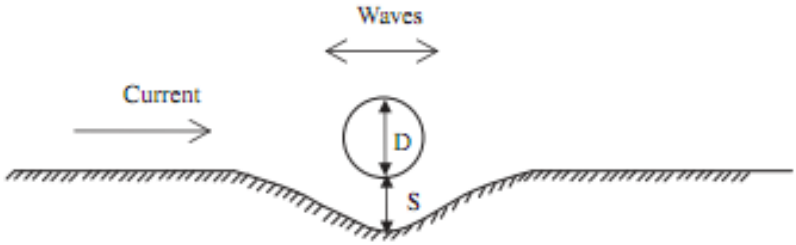

Figure 14: Definition sketch of scour depth S under pipeline, Myrhaug et al. (2009).

4.3 Waves plus current

Sumer and Fredsøe (1996) presented an experimental study of scour below a pipeline in irregular waves plus current for $5 < KC < 50$ and live-bed conditions. They found that Eq. (27) can be employed for irregular waves as well provided that the Keulegan-Carpenter number is calculated as KC_{SF} given in Eq. (25). Also, in this case $KC_{SF} = U_{rms}T_p/D$. They found that the following empirical expression can be employed to find the equilibrium scour depth below a pipeline in irregular waves plus current

$$\frac{S}{D} = \frac{S_{cur}}{D}F \tag{28}$$

where $\frac{S_{cur}}{D} = 0.6$ is the nondimensional scour depth with a nondimensional standard deviation of $\sigma/D = 0.2$ for the case of current alone, and F is a function of KC_{SF} and U_{cwrms} given by

$$F = \frac{5}{3}KC_{SF}^{a}\exp(2.3b) \quad \text{for} \quad 0 \leq U_{cwrms} \leq 0.7 \tag{29}$$

$$F = 1 \quad \text{for} \quad 0.7 \leq U_{cwrms} \leq 1 \tag{30}$$

where U_{cwrms} is given in Eq. (23). The coefficients a and b are given as:

1. For $0 \leq U_{cwrms} \leq 0.4$:

$$a = 0.557 - 0.912(U_{cwrms} - 0.25)^2 \tag{31}$$

$$b = -1.14 + 2.24(U_{cwrms} - 0.25)^2 \tag{32}$$

2. For $0.4 \leq U_{cwrms} \leq 0.7$:

$$a = -2.14U_{cwrms} + 1.46 \tag{33}$$

$$b = 3.3U_{cwrms} - 2.5 \tag{34}$$

It is noticed that there is a discontinuity in Eqs. (31), (33) and Eqs. (32), (34) at $U_{cwrms} = 0.4$. However, for the wave dominated case this is not an issue since $U_{cwrms} < 0.4$. For the case of waves alone, given as $U_{cwrms} = 0$, it appears that Eqs. (28), (29), (31) and (32) reduce to Eq. (27) if KC is replaced by KC_{SF}. The stochastic method presented here is based on the assumption that the formulas for irregular waves plus current can be employed for regular waves plus current as well given that U_{cwrms} and KC_{SF} is replaced by U_{cw} in Eq. (26) and KC, respectively. This assumption is identical to the case of the vertical pile. So, the dimensionless coeffisient F for regular waves plus current in a wave dominated seastate becomes

$$F = \frac{5}{3} KC^a \exp(2.3b) \quad \text{for} \quad 0 \leq U_{cw} \leq 0.4 \tag{35}$$

where the coefficients a and b are given by

$$a = 0.557 - 0.912(U_{cw} - 0.25)^2 \tag{36}$$

$$b = -1.14 + 2.24(U_{cw} - 0.25)^2 \tag{37}$$

5 Burial and scour of short cylinders

Understanding the interaction between a short cylinder and the seabed in waves or combined flows is of great interest for several applications. Mines at sea are often shaped like short cylinders and it is important that they are not buried or surrounded by a large scour hole in order to obtain maximum effect of the explosion. Apart from military use, this field is also of importance for geophysical and engineering purposes. Similar to the case of the vertical pile and the pipeline, the burial and scour process is governed by the KC-number.

5.1 Mechanisms

The process of scour around a short cylinder can be devided into the same stages as for the case of the long pipeline described in Section 4.1.1, namly onset of scour, tunnel erosion, lee wake erosion and equilibrium stage. In wave dominated seastates the KC-number is still the crucial parameter in the incoming flow. First, the onset of scour takes place around the ends of the cylinder due to the local increase in velocity, Catano-Lopera and Garcia (2006). Next, the tunnel erosion takes over at the ends and the onset of scour moves towards the center of the cylinder from both sides causing a decrease in the area of the seabed supporting the body. After a certain amount of time the weight of the body exceeds the bearing capacity of the seabed and the body sinks until equilibrium is restored. This process continues until the equilibium state is reached, defined as $\alpha = 1$ from Eq. (1). Fig. 15 shows how the suppporting seabed is eroded away by two advancing fronts of scour. The lee-wake vortices caused by the back and forth motion of the waves will transport seabed sediments away from the cylinder during each half wave periode, resulting in a scour hole. Even for waves alone, experiments by Catano-Lopera and Garcia (2007) show that the downstream length of the scour hole will be longer than the upstream counterpart. This effect is due to nonlinearities in the seastate.

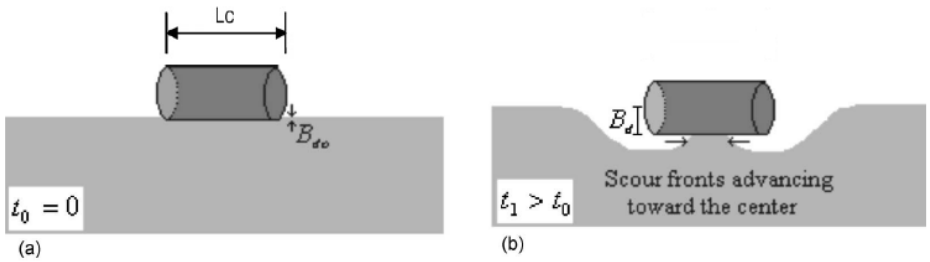

Figure 15: Burial B_d at initial stage, (a) and further into the process,(b) , Catano-Lopera and Garcia (2006).

5.2 Regular waves plus current

5.2.1 Burial

Catano-Lopera and Garcia (2006) presented experimental data from laboratory tests of burial of short cylinders under combined regular waves and current. For a circular cylinder with diameter D and length L_c they found that the equilibrium burial depth B_d, defined in Fig. 15, is given by the empirical expression for live-bed conditions

$$\frac{B_d}{D} = c_1 \frac{U_m}{U_m + U_c} (\theta KC)^{c_2} \tag{38}$$

where

$$(c_1, c_2) = (0.24, 0.4) \tag{39}$$

The experiments were performed for aspect ratios $a_r = L_c/D$ in the range of 2 to 4 and for Keulegan-Carpenter numbers in the range 2 to 48. Further, Eq. (38) is based on waves alone ($U_c = 0$) and two seastates with additional current corresponding to $U_m/(U_m + U_c) = (1, 0.8, 0.79)$. In terms of U_{cw} this corresponds to $U_{cw} = (0, 0.2, 0.21)$, which is well within the wave dominant region.

5.2.2 Scour

Catano-Lopera and Garcia (2007) investigated the scour around a short cylinder in regular waves plus current through laboratory tests and found the following empirical expression for the equilibrium scour hole length L

$$\frac{L}{D} = p_1 KC^{p_2} \tag{40}$$

L can represent the total length of the scour hole L_{st} or the downstream length of the scour hole L_{sd} dependent on p_1 and p_2. For each representation of L the coefficients are given as

- $L = L_{sd}$ gives $(p_1, p_2) = (0.75, 0.56)$
- $L = L_{st}$ gives $(p_1, p_2) = (0.75a_r^3, 0.6)$

L_{st}, L_{sd} and L_{su} are defined in Fig. 16. The upstream length of the scour hole can be calculated as $L_{su} = L_{st} - L_{sd}$. The width of the scour hole W was found to be independent of

KC and ranging from $1.3L_c$ to $2.5L_c$ with a mean value of $1.8L_c$. It should be noted that Eq. (40) is valid for live-bed conditions and does not accound for current effects. The equilibrium length is based on KC in the range of 2 to 71 and the aspect ratio a_r in the range of 2 to 4. Even though Eqs. 40 and 38 are continous for all $KC \geq 0$, it should be noted that this may not be physically correct as the threshold for the scour mechanism may not be exceeded for the smallest values of KC. However, since the highest waves are responsible for the better part of the scour response the effect from any lower threshold value in KC is neglected.

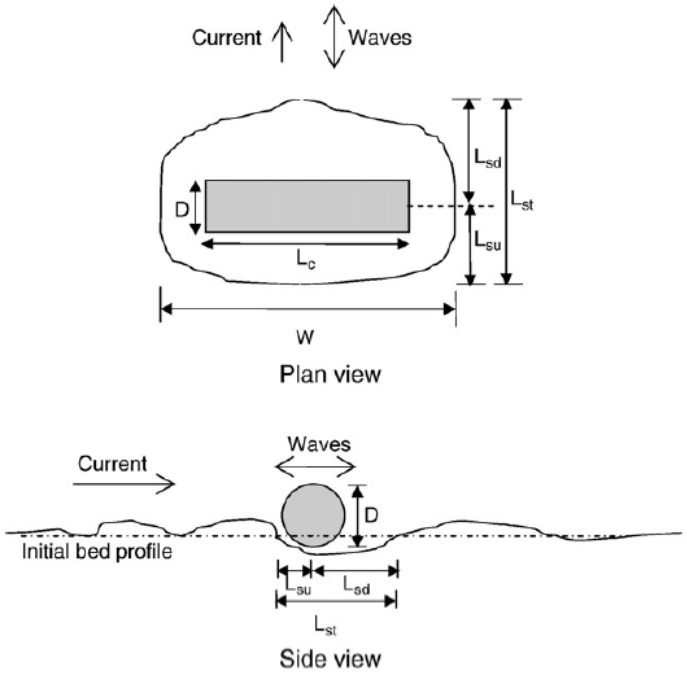

Figure 16: Definitions of L_{st}, L_{sd} and L_{su} for the scour hole geometry around a short cylinder, Myrhaug and Ong (2009).

6 Scour in nonlinear random waves

6.1 Nonlinear waves

In order to say something about the scour depth the KC-number at the seabed must be assessed. The maximum free surface elevation in a sea state with stationary narrowband waves consistent with Stokes second order can be described as, Myrhaug (2006)

$$\eta_c = a + \frac{1}{4} k_p a^2 \frac{\cosh(k_p h)}{\sinh^3(k_p h)} (2 + \cosh(2k_p h)) \tag{41}$$

where a is linear wave amplitude, k_p is the wavenumber corresponding to the peak frequency ω_p given by the dispersion relationship

$$\omega_p^2 = g k_p \tanh k_p h \tag{42}$$

For simplicity Eq. (41) is rewritten into

$$\eta_c = a + \frac{1}{2} k_p a^2 b(k_p h) \tag{43}$$

where

$$b(k_p h) = \frac{\cosh(k_p h)(2 + \cosh(2k_p h))}{2\sinh^3(k_p h)} \tag{44}$$

The crest height is made dimensionless by evaluating $w_c = \eta_c / a_{rms}$ where a_{rms} is the rms value of the linear wave amplitude.

$$w_c = \hat{a} + \frac{1}{2} \hat{a}^2 k_p a_{rms} b(k_p h) \tag{45}$$

where $\hat{a} = \frac{a}{a_{rms}}$. If the terms of second order are assembeld into $O(k_p a_{rms})$ the following expression is obtained

$$w_c = \hat{a} + O(k_p a_{rms}) \tag{46}$$

where $k_p a_{rms}$ denotes the characteristic wave steepness of the sea state.
The maximum horizontal velocity evaluated at the seabed using Stokes second order theory is, Myrhaug (2006)

$$U_m = a \frac{\omega_p}{\sinh k_p h} + \frac{3}{4} a^2 \omega_p k_p \frac{1}{\sinh^4 k_p h} \tag{47}$$

By multiplying the right hand side of Eq. (47) with a_{rms}/a_{rms} and gathering the terms of second order into $O(k_p a_{rms})$ the following expression is obtained.

$$U_m = \hat{a} \frac{\omega_p a_{rms}}{\sinh k_p h} + O(k_p a_{rms}) \tag{48}$$

By dividing with the rms value of U_m the nondimensional nonlinear maximum horisontal particle velocity at the seabed is found as U_m / U_{rms}

$$\hat{U}_m = \frac{U_m}{U_{rms}} \hat{a} + O(k_p a_{rms}) \tag{49}$$

where

$$U_{rms} = \frac{\omega_p a_{rms}}{\sinh k_p h} \tag{50}$$

The corresponding rms value of the Keulegan-Carpenter number for a narrowbanded seastate is given by U_{rms} and T_p

$$KC_{rms} = \frac{U_{rms} T_p}{D} \tag{51}$$

Inverting Eq. (46) gives $\hat{a} = w_c - O(k_p a_{rms})$ and substituting into Eq. (49) gives $\hat{U}_m = w_c + O(k_p a_{rms})$. Consequently, w_c can replace $\hat{a}$ in the linear part of $\hat{U}_m$ because the error involved is of second order. By neglecting the terms of $O(k_p a_{rms})$ it appears that $\hat{U}_m = w_c$ involving that the same probability density function structure can be utilized. Moreover, the maximum horizontal water particle velocity evaluated at the seabed is found by replacing a_{rms} with η_c in Eq. (50)

$$U_m = \frac{\omega_p \eta_c}{\sinh k_p h} \tag{52}$$

Moreover,

$$A_{rms} = \frac{U_{rms}}{\omega_p} = \frac{a_{rms}}{\sinh k_p h} \tag{53}$$

by using Eq. (50).

6.2 Forristall distribution

For nonlinear waves the orbital velocity near the seabed is larger in the wave progation direction than in the oposite direction. In terms of scour, this effect was investigated by Catano-Lopera and Garcia (2007) through experiments. Myrhaug et al. (2009), among others, presented a stochastic model for predicting scour below second order Stokes waves, including sum frequency effects only. In this report, the wave crest distribution presented by Forristall (2000) based on simulations of 2D and 3D waves using second order theory will be employed. He adapted a two-parameter Weibull distribution where the parameters were obtained by best fit to data for 2D and 3D waves including both sum-frequency and difference-frequency effects.
Fig. 17 is taken from Wist (2003) and shows the relative magnitude between sum-frequency and difference-frequency effects for varying depth and constant sum-frequency of $\omega_1 + \omega_2 = 1.12$ rad/s for 2D waves only. Fig. 18 shows a principal sketch of the total 2D and 3D waves with corresponding difference-frequency terms in finite and deep water. From Fig. 17 it appears that in large water depths the difference-freqeuncy effects are neglectible for 2D waves. Forristall (2000) states that the difference-frequency effects can be neglected in deep water for the case of 3D waves as well and that the sum-frequency effects for 3D waves are slighty reduced compared to 2D waves, causing the wave crest to become higher for 2D waves in deep water.

In Fig. 17 it appears that for $h \approx 16$m the difference-frequency effects have increased to the same order of magnitude as the sum-frequency effects, hence the difference-frequency terms can not be neglected in finite water depth. According to Forristall (2000) this is also the case for 3D waves. Further, the 3D waves have smaller difference-frequency effects than the 2D waves resulting in lower wave crests and deeper wave troughs for 2D waves. Alternativly; 2D waves have larger set-down effects than 3D waves in finite water depth. This is illustrated in Fig. 18.

The cumulative Forristall distribution is given by

$$P(w_c) = 1 - exp\left[-\left(\frac{w_c}{\sqrt{8}\alpha}\right)^{\beta}\right] \text{ for } w_c \geq 0 \tag{54}$$

where α and β are based on the steepness S_1 and Ursell number U_R defined as

$$S_1 = \frac{2\pi}{g}\frac{H_s}{T_1^2} \tag{55}$$

$$U_R = \frac{H_s k_1}{(k_1 h)^3} \tag{56}$$

Here T_1 is the mean spectral periode, H_S is the significant wave height and k_1 is the wave number corresponding to T_1. In this case the seastate is narrowbanded so it is reasonable to assume that $T_1 = T_P$ which implies that $k_1 = k_P$. From Fig. 17 it appears that the variations caused by changing the bandwidth are neglectible which supports this assumption. S_1 and

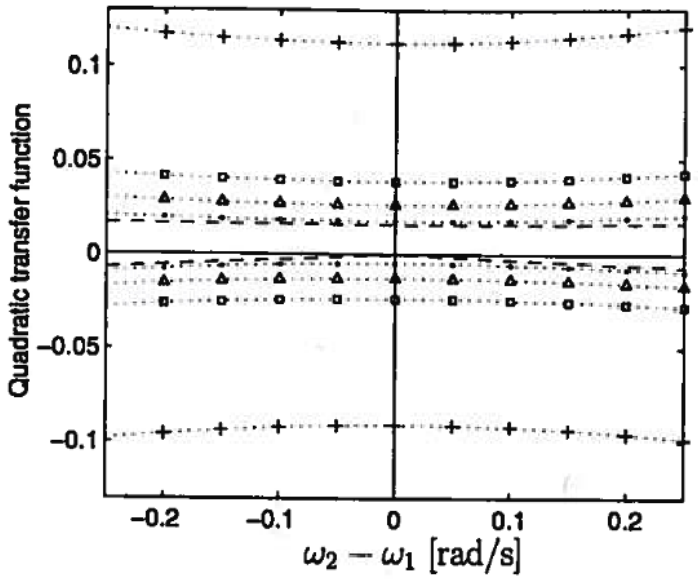

Figure 17: The quadratic transferfunction is a measure of the magnitude of sum-freqeuncy and difference-frequency effects. The positive values describes sum-frequency effects and negative values describes difference-frequency effects. $\omega_1 - \omega_2$ describes the bandwidth of the seastate. Valid for 2D waves. Waterdepths defined as: – deep water; $\cdot \bullet \cdot\cdot$ = 70 m; $\cdot \triangle \cdot\cdot$ = 42 m; $\cdot \square \cdot \cdot$ = 31 m; $\cdot + \cdot\cdot$ = 16 m. Wist (2003).

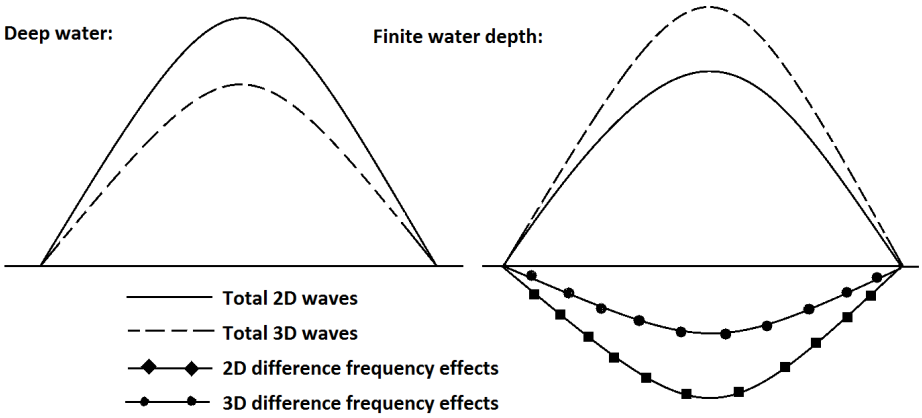

Figure 18: Principal sketch of difference-frequency effects and total height of wave crest

U_R describes the level of nonlinearity in the waves. For the case where $S_1 = 0$ and $U_R = 0$ the distribution is forced to match the Rayleigh distribution. For the 2D case the parameters are given by:

$$\alpha_{2D} = 0.3536 + 0.2892S_1 + 0.1060U_R \tag{57}$$

$$\beta_{2D} = 2 - 2.1597S_1 + 0.0968U_R^2 \tag{58}$$

and for the 3D case:

$$\alpha_{3D} = 0.3536 + 0.2568S_1 + 0.0800U_R \tag{59}$$

$$\beta_{3D} = 2 - 1.7912S_1 - 0.5302U_R + 0.2484U_R^2 \tag{60}$$

It should be noted that the Forristall distribution is based on simulations for $U_R \leq 1$. In the following calculations α and β will be employed to describe both the 2D and 3D case.

6.2.1 Truncated Forristall distribution

If w_c is defined within a limited interval $w_{c1} < w_c < w_{c2}$ then this is accounted for by letting w_c follow the truncated Forristall distribution given by

$$P(w_c) = \frac{\exp\left[-\left(\frac{w_{c1}}{\sqrt{8}\alpha}\right)^\beta\right] - \exp\left[-\left(\frac{w_c}{\sqrt{8}\alpha}\right)^\beta\right]}{\exp\left[-\left(\frac{w_{c1}}{\sqrt{8}\alpha}\right)^\beta\right] - \exp\left[-\left(\frac{w_{c2}}{\sqrt{8}\alpha}\right)^\beta\right]} \quad \text{for} \quad w_{c1} \leq w_c \leq w_{c2} \tag{61}$$

6.3 Expected value of scour

This stochastic approach for finding the scour depth in nonlinear random wave plus current is based the assumptions that the seastate has lasted longer than the timescale of the scour and that only the $1/n$'th highest waves contribute to scour response. Also, the method is valid for live-bed conditions. The highest waves are exceeded by a probability of $1/n$ and the corresponding value for w_c is denoted $w_{c1/n}$. This quantity is found by solving $1 - P(w_{c1/n}) = 1/n$. The expected equilibrium scour depth caused by the $1/n$'th highest wave crests is then given by

$$E[S(w_c)|w_c > w_{c1/n}] = n \int_{w_{c1/n}}^{\infty} S(w_c)p(w_c)dw_c \tag{62}$$

where $p(w_c)$ is the probability density function and $S(w_c)$ is the equilibrium scour depth given by w_c which will be elaborated further in the following sections. This method is based on two main assumptions:

- The free surface elevation is a stationary narrowband random process with an expectation value of zero
- The formulas for scour depth in regular waves plus current provided in the previous sections are valid for irregular waves plus current as well

In order to investigate the ratios between expected equilibrium scour depth predicted by 3D, 2D and linear waves it is appropriate to give R_1(3D waves) as the ratio between 3D and linear waves, R_1(2D waves) is the ratio between 2D and linear waves and R_2 is the ratio between 3D and 2D waves.

6.3.1 Ursell criterion

It should be noted that since the Forristall distribution is only given for $U_R \leq 1$ there are certain limitations. For a given value of H_s and h the lower limit of k_p can be found from Eq. (56) by solving for k_p. The peak frequency ω_p is found from the dispersion relationship in Eq. (42) and the corresponding rms value of the maximum horizontal particle velocity evaluated at the seabed U_{rms} is found in Eq (50). Recalling the rms value of the Keulegan-Carpenter number in Eq. (24) it appears that there is an upper limit in KC_{rms} if the diameter D is given. This must kept in mind, regardless of what type scour that is considered. As an example; if a structure with diameter $D = 1$m on the seabed (vertical pile, pipeline or short cylinder) is exposed to waves with $H_s = 3$m and waterdepth $h = 10$m, the resulting upper limit will be $KC_{rms} = 11.59$. This example is most suitable for vertical piles or pipelines as the short cylinders often have smaller diameter. For a sea mine (short cylinder) with $D = 0.2$m the corresponding limit is $KC_{rms} = 57.95$. For future applications this will be refered to as the Ursell criterion.

6.3.2 Forristall effect due to change of structure diameter

When regarding 2D or 3D waves it is important to be aware of that S_1 and U_R determines the shape of $p(w_c)$ through α and β. As mentioned S_1, U_R are measures of the degree of nonlinearity in the seastate and KC_{rms} contains information about the wave action relative to the diameter of the structure. A connection between these three quantities will now be elaborated. By inserting the expression for U_{rms} from Eq. (50) into Eq. (51) and recalling that $\omega_p = 2\pi/T_p$ the new expression becomes

$$KC_{rms} = \frac{2\pi a_{rms}}{D \sinh k_p h} \tag{63}$$

For a given a_{rms}, h and KC_{rms} it appears that any variations in the diameter must be compensated for by the wave number k_p. So far, this is the case for linear waves as well. For 2D or 3D waves the variation in k_p will cause changes in the pdf as α and β are indirectly dependent on k_p. This means that if the seastate and the Keulegan-Carpenter number are given the expected equilibrium scour depth in Eq. (62) will vary with the diameter of the structure. Fig. 30 in Appendix A illustrates this effect. This is not an issue for linear waves since $S_1 = 0$ and $U_R = 0$. The common practice in the previously mentioned works is to present the expected equilibrium scour depth as S/D but here this can be misleading as the Forristall distribution is employed in this report. In order to avoid confusion the results of expected scour respons by linear, 2D and 3D waves in the following sections will mainly be given with dimension in meters along the y-axis and specified characteristic diameter on top. For future applications this will be referred to as the Forristall effect.

6.4 Shields parameter

The task of finding the Shields parameter in random waves may offer some challenges as it is not obvious which value of θ that actually corresponds to live-bed scour. Recalling that the scour depth was determined as the expected scour response from the $1/n$'th largest waves, the Shields parameter must be assessed in a corresponding manner. In the following, a method for calculating the Shields parameter in 3D, 2D and linear random waves will be described.

First, the dimensionless Shields parameter θ_c is given as $\theta_c = \theta_m/\theta_{rms}$. From the definition of θ in Eq. (3) it appears that θ_c is equal to the non-dimensional maximum bottom shear stress under the waves crest for individual random waves $\tau_c = \tau_m/\tau_{rms}$. θ_{rms} is defined as

$$\theta_{rms} = \frac{\tau_{rms}}{\rho g(s-1)d_{50}} \tag{64}$$

where τ_{rms} is given by

$$\tau_{rms} = \frac{1}{2}c\left[\frac{A_{rms}}{z_0}\right]^{-d} U_{rms}^2 \tag{65}$$

θ_m can by found by replacing τ_{rms} with τ_m in Eq. (64). Myrhaug and Holmedal (2011) proposed a model for calculating bottom friction beneath 2D and 3D random waves for different flow regimes. For rough turbulent flow they stated that $\tau_c = w_c^{2-d}$. Recalling that $\tau_c = \theta_c$ gives

$$\theta_c = w_c^{2-d} \tag{66}$$

Now the expected value of the nondimensional Shields parameter can be found by employing the incomplete gamma function $\Gamma(:,:)$ (further described in Myrhaug et al. (2009)).

$$E[\theta_c(w_c)|w_c > w_{c1/n}] = n\left(\sqrt{8}\alpha\right)^{2-d}\Gamma\left[1+\frac{2-d}{\beta}, \ln n\right] \tag{67}$$

For the case of linear waves $\alpha = 1/\sqrt{8}$ and $\beta = 2$.

7 Vertical pile in nonlinear random waves plus current

7.1 Method

Now a stochastic method for finding the equilibrium scour depth around a single vertical circular pile in nonlinear random waves plus current will be shown. For the case of random waves, the KC-number in Eq. (11) is found employing $U_m = w_c U_{rms}$ which gives

$$KC = w_c KC_{rms} \tag{68}$$

Based on this, Eq. 13 can be rearranged to find the equilibrium scour depth due to narrowband random waves plus current as

$$S = DC(1-\exp[-q(KC_{rms}w_c - r)]) \quad \text{for} \quad w_c \geq w_{cl} = \frac{r(w_c)}{KC_{rms}} \tag{69}$$

where w_{cl} is the lower limit for w_c as a consequence of that Eq. (13) is valid for $KC \geq r$. q and r are given by

$$q = 0.03 + 0.75U_{cw}^{2.6} \tag{70}$$

$$r = 6\exp(-4.7U_{cw}) \tag{71}$$

where

$$U_{cw} = \frac{U_{cr}}{U_{rms}w_c + U_{cr}} \tag{72}$$

Thus, $P(w_c)$ is the truncated cumulative Forristall distribution described in Eq (61) with $w_{c1} = w_{cl}$ and w_{c2} approaching an infinitly large value.

$$P(w_c) = \frac{\exp\left[-\left(\frac{w_{cl}}{\sqrt{8}\alpha}\right)^{\beta}\right] - \exp\left[-\left(\frac{w_c}{\sqrt{8}\alpha}\right)^{\beta}\right]}{\exp\left[-\left(\frac{w_{cl}}{\sqrt{8}\alpha}\right)^{\beta}\right]} \tag{73}$$

The $1/n$'th largest values of w_c is then given by solving $1 - P(w_{c1/n}) = 1/n$.

$$w_{c1/n} = \sqrt{8}\alpha\left[\left(\frac{w_{cl}}{\sqrt{8}\alpha}\right)^{\beta} + \ln n\right]^{1/\beta} \tag{74}$$

The probability density function of w_c is found by evaluating $p(w_c) = dP/dw_c$

$$p(w_c) = \left(\frac{1}{\sqrt{8}\alpha}\right)^{\beta}\beta w_c^{\beta-1}\exp\left[\left(\frac{w_{cl}}{\sqrt{8}\alpha}\right)^{\beta} - \left(\frac{w_c}{\sqrt{8}\alpha}\right)^{\beta}\right] \tag{75}$$

The expected value of the scour depth is found by evaluating the integral in Eq. (62). However, it should be noticed that the lower limit of the integration, $w_{c1/n}$, is dependent on the lower limit of the probability density function. In order to ensure correct contribution from all values of w_c in the integration the Heaviside function must be employed. It is defined as

$$H(w_c - w_{c1/n}) = \begin{cases} 1 & \text{if } w_c > w_{c1/n} \\ 0 & \text{if } w_c < w_{c1/n} \end{cases}$$

So, the expected equilibrium scour depth around a single vertical pile caused by the $1/n$'th largest waves based on Eq. (62) is found as

$$E[S(w_c)|w_c > w_{c1/n}] = n\int_0^{\infty} S(w_c)p(w_c)H(w_c - w_{c1/n})dw_c \tag{76}$$

The stochastic method for finding the equilibrium scour depth around single vertical piles with square cross sections and the group arrangements of piles in nonlinear random waves is equal to the method presented in this section, except that the coefficients (C, q, r) are given in Eqs (15)-(16) and Eqs (18)-(20). Due to the fact that the current velocity is not accounted for in the latter cases (r and q are constants) the stochastic method becomes less complicated. The lower limit for the truncated Forristall distribution is $w_{cl} = r/KC_{rms}$ and the expected equilibrium scour depth around a square pile or a group of piles can now be written as

$$E[S(w_c)|w_c > w_{c1/n}] = n\int_{w_{c1/n}}^{\infty} S(w_c)p(w_c)dw_c \tag{77}$$

where $S(w_c)$, $w_{c1/n}$ and $p(w_c)$ are given in Eqs. (69), (74) and (75), respectivly.

7.2 Results

All the plots presented in this section are given with dimension for a spescific pile diameter of $D = 1$m. For the linear waves, this involves that the expected equilibrium scour depth can be understood as S/D and that the results are valid for any other pile diameter within

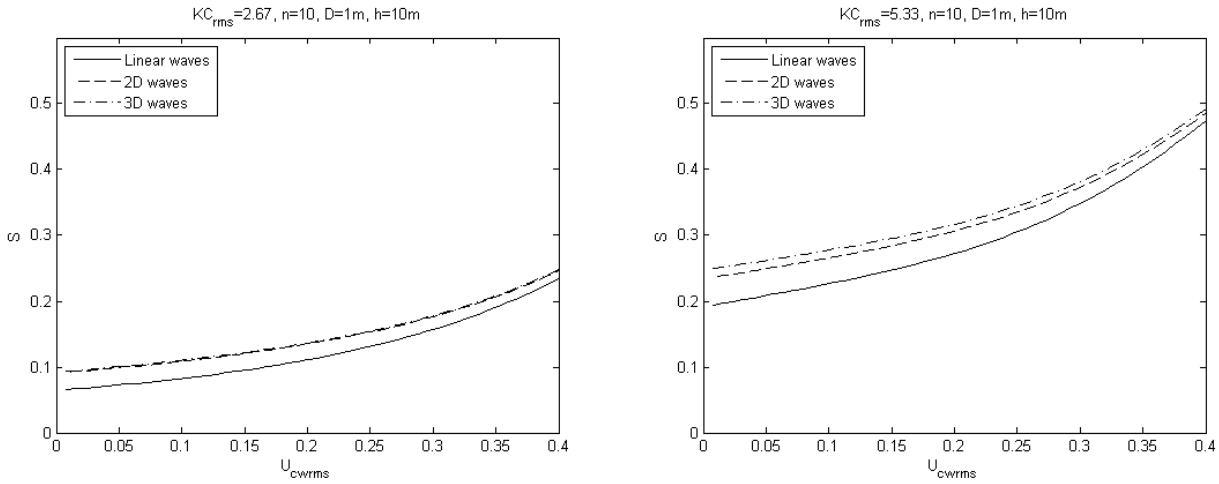

(a) $KC_{rms} = 2.67$ (b) $KC_{rms} = 5.33$

Figure 19: Expected scour depth for linear, 2D and 3D random waves around a vertical circular pile versus U_{cwrms}

the slender pile regime. However, due to the previously mentioned Forristall effect in Section 6.3.2, this is not the case for 3D and 2D waves. The seastate is given by $H_s = 3$m and $h = 10$m and, consequently, the upper limit in KC_{rms}, based on the Ursell criterion is 11,59. Further, it is assumed that only the 1/10'th largest wave crests will contribute to the scour respons, hence $n = 10$. Additional results for piles can be found in Appendix A.

7.2.1 Circular cross section

Myrhaug et al. (2009) compared the predictions from the stochastic model for linear random waves ($\alpha = 1/\sqrt{8}, \beta = 2$) and the measured data presented by Sumer and Fredsøe (2001) for for co-directional waves plus current versus U_{cwrms} in the range of $0 - 0.4$ for $n = (3, 10)$ and with $KC_{rms} = (2.67, 5.33, 17.33)$ in their Fig. 4. Fig. 19 in this report illustrates the corresponding results for S based on linear, 2D and 3D waves. As expected, it appears that the nondimensional expected scour depth in Myrhaug et al. (2009) is equal to the expected scour depth in Fig. 19 given by the linear waves as $D = 1$m. Due to the Ursell criterion, only the plots for $KC_{rms} = (2.67, 5.33)$ are of interest.

It appears that the 2D and 3D waves cause more scour compared to the linear waves over the entire range of current velocity and for both values of KC_{rms}. Also, the scour depth increases for increasing current velocity. For $KC_{rms} = 2.67$ the 2D and 3D waves will cause about the same amount of scour but for $KC_{rms} = 5.33$ the 3D waves will dominate.

Fig. 20 illustrates the ratios of scour depth as a function of KC_{rms} for $U_{cwrms} = 0.2$. It appears that 2D and 3D waves induce more scour than linear waves for all KC_{rms}. The reason for the sudden increase in R_1 (2D waves) and R_1 (3D waves) at $KC_{rms} \approx 2$ is due to low scour response from linear waves. For $KC_{rms} \gtrsim 2$ the 3D waves induce more scour than 2D waves whereas for lower KC_{rms} the 2D waves will generate more scour.

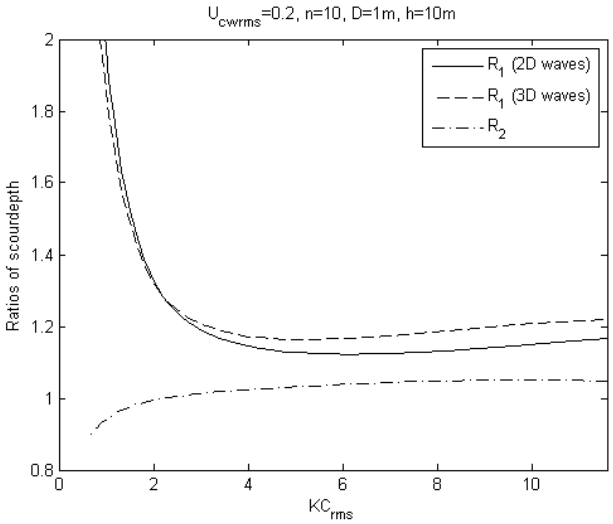

Figure 20: Ratios of scour depth around vertical circular pile versus KC_{rms}.

7.2.2 Square cross section

Fig. 21 illustrates the ratios of scour depth around a 45° and 90° square pile in random waves as a function of KC_{rms} for 3D, 2D and linear random waves.

For both the 45° and 90° square pile it appears that 2D and 3D waves induce more scour than linear waves for all KC_{rms}. Further, for the lowest values of KC_{rms} the scour response from 2D waves is largest, but when $KC_{rms} \gtrsim 2$ the 3D will cause the largest scour depth. This effect is more distinguished for the 90° square pile.

7.2.3 Groups of piles

Figs. 22 and 23 illustrate the ratios of scour depth around the side-by-side, 45° staggered and the 4×4 arrangement of piles in random waves for $G/D = 0.4$ versus KC_{rms} for 3D, 2D and linear random waves. The two-pile arrangements have similar ratios as the single circular pile in Fig. 20 whereas the 4×4 arrangement has many common features with the 90° square pile in Fig. 21b which seems reasonable due to the square shape of the arrangement.

7.3 Example of calculation of scour

The purpose of this example is to show the application of the stochastic method for a single circular vertical pile. The flow conditions are taken from the corresponding example in Myrhaug et al. (2009) and given by:

- Water depth, $h = 10$m
- Significant wave height, $H_s = 3$m
- Spectral peak periode, $T_p = 7.9$s corresponding to $\omega_p = 0.795$ rad/s
- Median grain diameter, $d_{50} = 1$mm
- $s = 2.65$ (quartz sand)

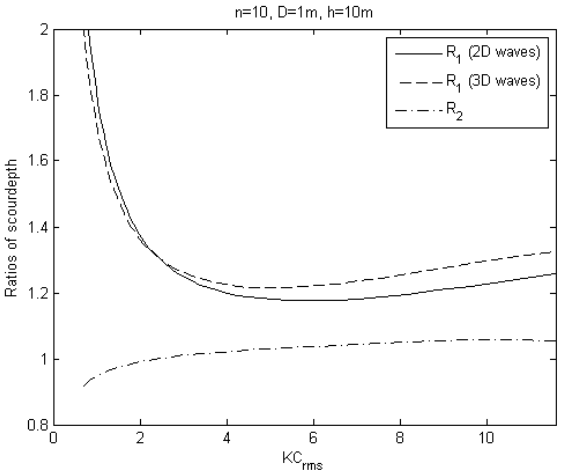

(a) 45°

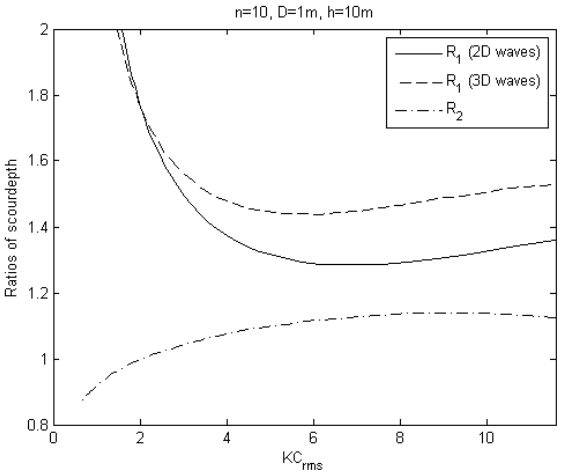

(b) 90°

Figure 21: Ratios of scour depth for square piles versus KC_{rms}

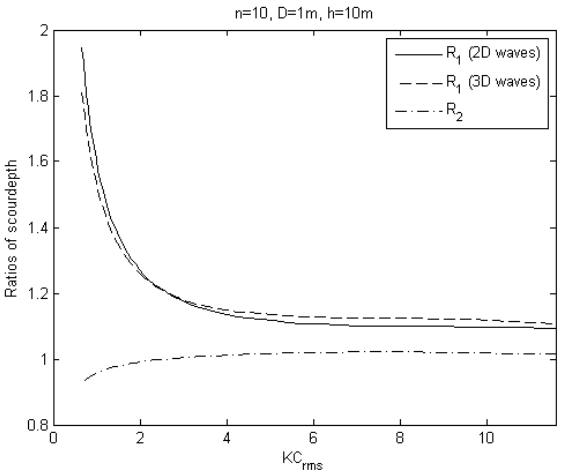

(a) Side-by-side

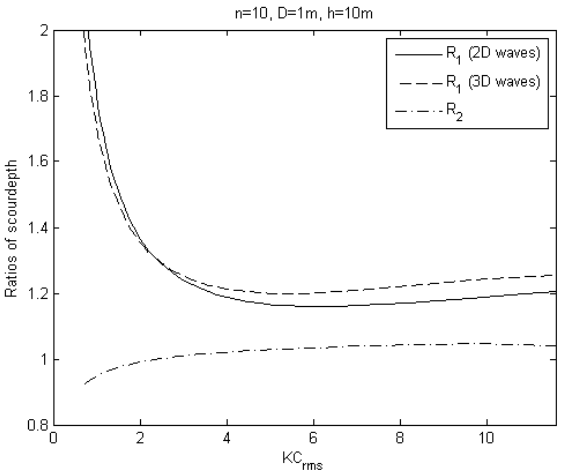

(b) 45° staggered

Figure 22: Ratios of scour depth for two-pile arrangements versus KC_{rms}

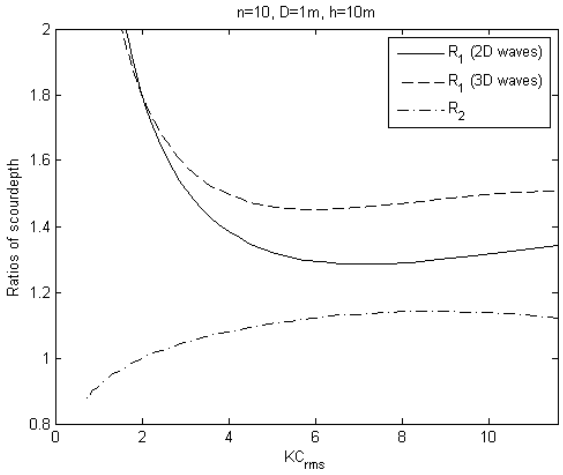

Figure 23: Ratios of scour depth around 4×4 arrangement of piles versus KC_{rms}.

- Current speed, $U_c = 0.2$m/s

- $n = 10$

Table 1 presents the calculated values which are independent of the diameter of the pile which involves that they are valid for other cases of scour as well. The *rms* value of the wave amplitude is calculated as $a_{rms} = H_s/2\sqrt{2}$. Further, as the seastate is assumed to be narrowbanded the values for S_1 and U_R (see Eqs. (55) and (56), respectivly) are obtained by substituting T_1 and k_1 with T_p and k_p, respectivly. $U_R < 1$ meaning that the flow condition is within the validity range of the Forristall distribution. As $U_{cwrms} = 0.196$ it follows that the seastate is wave dominated. $U_{rms}/(U_{rms} + U_c) = 0.804$ is given as the this flow condition also will be employed for the short cylinder. Recalling that $z_0 = d_{50}/12$ involves that A_{rms}/z_0 exceeds 11,000 and, consequently, the coefficients $(c, d) = (0.112, 0.25)$. θ_{rms} exceeds θ_{cr} which results in live-bed conditions. The largest maximum Shields parameter is caused by 3D waves, followed by 2D and linear waves. So far, calculations are independent of the characteristic diameter of the structure.

The resulting scour depths S from linear, 2D and 3D waves around a vertical pile with a diameter of $D = 0.3$m (taken from corresponding example in Myrhaug et al. (2009)) and $C = 1.3$ are given in Table 2. Regardless of the presence of current, the nonlinear waves will induce a larger scour depth than linear waves. The 3D waves causes the largest scour depth closely followed by 2D waves. This is due to smaller set-down effects for 3D waves than 2D in finite water depth as discussed in Section 6.2. For waves alone, the ratios $S_{nonlin,3D}/S_{lin} = 1.114$ and $S_{nonlin,2D}/S_{lin} = 1.093$. For waves plus current, the ratios become $S_{nonlin,3D}/S_{lin} = 1.078$ and $S_{nonlin,2D}/S_{lin} = 1.066$ and it appears that the scour depth will increase compared to waves alone. Fig. 19 displays similar features.

Table 1: Example of calculation

a_{rms} (m)	1.06
k_p (rad/m) Eq. (42)	0.090
S_1 Eq. (55)	0.030
U_R Eq. (56)	0.370
α_{2D},β_{2D} Eqs. (57),(58)	0.4018,1.9468
α_{3D},β_{3D} Eqs. (59),(60)	0.3911,1.7874
A_{rms} (m) Eq. (53)	1.033
U_{rms} (m/s) Eq. (50)	0.821
U_{cwrms} Eq. (23)	0.196
$U_{rms}/(U_{rms}+U_c)$	0.804
A_{rms}/z_0	12399
c, d Eq. (10)	0.112,0.25
θ_{rms} Eqs. (64) and (65)	0.2214
Shields parameter; $\theta_m = \theta_c\theta_{rms}$	
θ_{clin} Eq. (67)	2.832
θ_{mlin}	0.627
$\theta_{cnonlin2D}$ Eq. (67)	3.647
$\theta_{mnonlin2D}$	0.807
$\theta_{cnonlin3D}$ Eq. (67)	3.840
$\theta_{mnonlin3D}$	0.850

Table 2: Scour depth around single circular pile with $D = 0.3$m

KC_{rms} Eq. (51)	21.629
Waves alone:	
S_{lin} (m)	0.245
$S_{nonlin,2D}$ (m)	0.268
$S_{nonlin,3D}$ (m)	0.273
Waves plus current:	
S_{lin} (m)	0.269
$S_{nonlin,2D}$ (m)	0.287
$S_{nonlin,3D}$ (m)	0.290

8 Pipeline in nonlinear random waves plus current

8.1 Method

The stochastic method for finding the equilibrium scour depth below a marine pipeline is very much similar to that of the vertical pile described in Section 7. The seastate is still assumed to be stationary narrowbanded and the formulas for regular waves plus current are assumed to be valid for irregular waves plus current as well. By employing Eqs. (68) the dimensional scour depth can be re-arranged to

$$S = D\frac{S_{cur}}{D}F \tag{78}$$

where F is given as

$$F = \frac{5}{3}(KC_{rms}w_c)^a \exp(2.3b) \tag{79}$$

The coefficients a and b are then given as

$$a(w_c) = 0.557 - 0.912(U_{cw} - 0.25)^2 \tag{80}$$

$$b(w_c) = -1.14 + 2.24(U_{cw} - 0.25)^2 \tag{81}$$

where U_{cw} is given in Eq. (72). Recalling that Eq. (35) is valid for $0 \leq U_{cw} \leq 0.4$, corresponds to the following requirement for w_c

$$w_c \geq w_{cl} = 1.5\frac{U_c}{U_{rms}} \tag{82}$$

Now the cumulative density function $P(w_c)$, the value of w_c which is exceeded with a probability $1/n$,$w_{c1/n}$, and the probability density function $p(w_c)$ are identical to those for the vertical pile and given in Eqs. (73) - (75) respectivly. However, w_{cl} is given in Eq. (82) for the pipeline.
The expected equilibrium scour depth caused by the $1/n$'th largest waves follows from Eq. (62) as

$$E[S(w_c)|w_c > w_{c1/n}] = n\int_{w_{c1/n}}^{\infty} S(w_c)p(w_c)dw_c \tag{83}$$

8.2 Results

Myrhaug et al. (2009) compared the predictions from the stochastic model for linear random waves ($\alpha = 1/\sqrt{8}, \beta = 2$) and the measured data presented by Sumer and Fredsøe (1996) for waves plus current versus U_{cwrms} in the range of $0 - 0.4$ for $n = (3, 10)$ and $KC_{rms} = (3.67, 6.67, 12, 26, 34, 7)$ in their Fig. 3. Fig. 24 in this report illustrates the corresponding results for S based on linear, 2D and 3D random waves. The seastate is given by $H_s = 3$m and $h = 10$m. As expected, it appears that the nondimensional expected scour depth in Myrhaug et al. (2009) is equal to the expected scour depth in Fig. 24 given by the linear waves as $D = 1$m. Further, this involves that the expected equilibrium scour depth given by linear waves can be understood as S/D and that the results are valid for any other pipeline diameter. However, due to the previously mentioned Forristall effect in Section 6.3.2, this is not the case for 3D and 2D waves. Equivalent to the case of the vertical piles the upper limit in

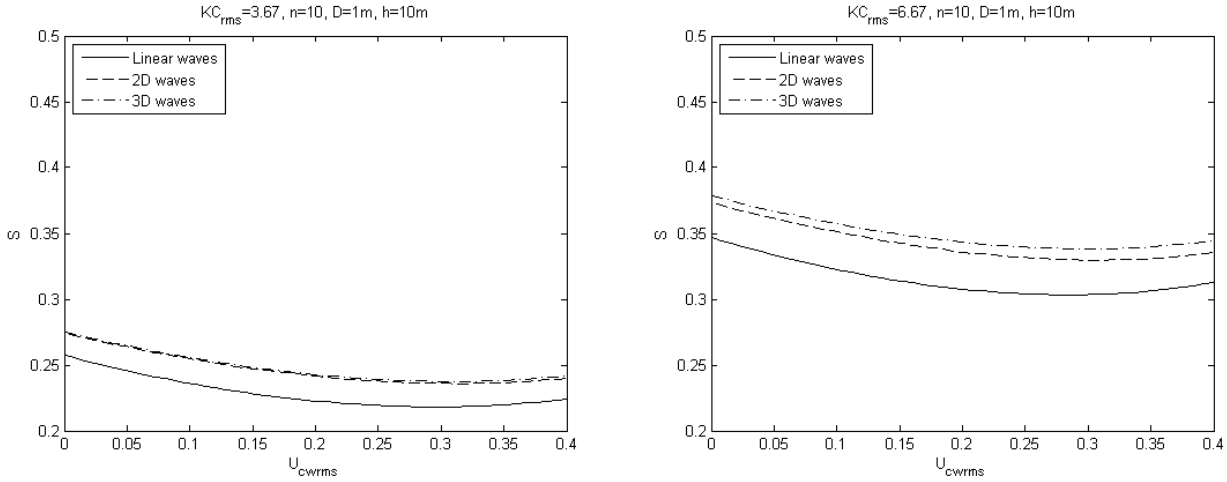

(a) $KC_{rms} = 3.67$ (b) $KC_{rms} = 6.67$

Figure 24: Expected scour depth for linear, 2D and 3D random waves around a pipeline versus U_{cwrms}

KC_{rms} is 11.59, based on the Ursell criterion. Hence, only the plots for $KC_{rms} = (3.67, 6.67)$ are of interest.

It appears that the 2D and 3D waves cause more scour compared to the linear waves over the entire range of current velocity and for both values of KC_{rms}. The variations with U_{cwrms} are very small, allthough it appears that the current will reduce the scour depth slightly compared to waves alone. For $KC_{rms} = 3.67$ the 2D and 3D waves will cause about the same amount of scour but for $KC_{rms} = 6.67$ the 3D waves will dominate.

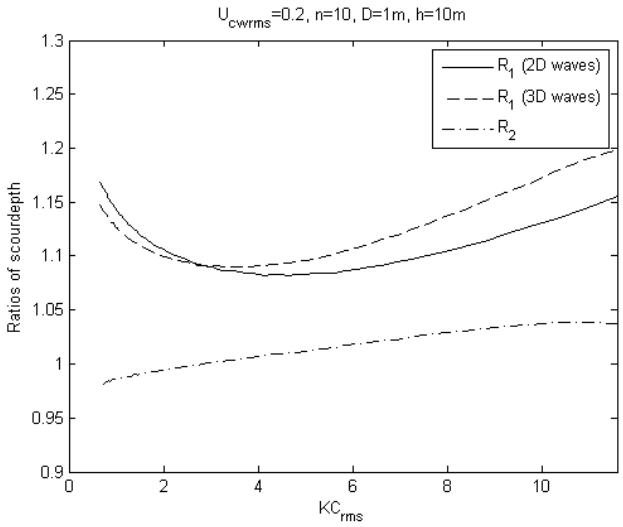

Figure 25: Ratios of scour depth around pipeline versus KC_{rms}.

Fig. 25 illustrates the ratios of scour depth as a function of KC_{rms} for $U_{cwrms} = 0.2$. It appears that 2D and 3D waves induce more scour than linear waves for all KC_{rms}. The

reason for the sudden increase in R_1 (2D waves) and R_1 (3D waves) at $KC_{rms} \lesssim 2$ is due to low scour response from linear waves. For $KC_{rms} \gtrsim 2$ the 3D waves induce more scour than 2D waves whereas for lower KC_{rms} the 2D waves will generate more scour. Additional results for pipelines and short cylinders can be found in Appendix B.

8.3 Example of calculation of scour depth under a pipeline

The following example of calculation of the scour depth under a pipeline is presented in order to demonstrate the application of the method and based on the same flow condition as the vertical pile described in Table 1

Table 3: Marine pipeline with $D = 0.3$m and flow conditions given in Table 1

KC_{rms} Eq. (51)	21.629
Waves alone:	
S_{lin} (m)	0.187
$S_{nonlin,2D}$ (m)	0.201
$S_{nonlin,3D}$ (m)	0.203
Waves plus current:	
S_{lin} (m)	0.174
$S_{nonlin,2D}$ (m)	0.189
$S_{nonlin,3D}$ (m)	0.193

The resulting scour depths S from linear, 2D and 3D waves under a marine pipeline with a diameter of $D = 0.3$m (taken from corresponding example in Myrhaug et al. (2009)) are given in Table 3. Similar to the case of the vertical pile, the nonlinear waves will induce a larger scour depth than linear waves. The 3D waves causes the largest scour depth closely followed by 2D waves. This is due to smaller set-down effects for 3D waves than 2D in finite water depth as discussed in Section 6.2. For waves alone, the ratios $S_{nonlin,3D}/S_{lin} = 1.085$ and $S_{nonlin,2D}/S_{lin} = 1.074$ which is slightly lower than the corresponding values for the vertical pile. For waves plus current, the ratios become $S_{nonlin,3D}/S_{lin} = 1.109$ and $S_{nonlin,2D}/S_{lin} = 1.086$; slightly higher the values for the vertical pile. Moreover, it appears that the current causes the scour depth to decrease. Fig. 24 displays similar features. The main mechanism of scour under a pipeline for waves alone is the lee-wake vortex system that occurs on both sides of the pipe. When the current is added this vortex system will be more violent on the downstream side of the pipeline compared to the upstream counterpart which results in a decrease in the scour depth underneath the pipeline. From Table 2 it appears that adding a current has the oposite effect on the scour depth around the vertical pile. The presence of a current will cause amplification of the horseshoe votices on the upstream part of the pile, resulting in a larger scour depth, Sumer and Fredsøe (2002).

9 Short cylinder in nonlinear random waves plus current

The stochastic method for finding the equilibrium burial depth and scour hole geometry is very much similar to that of the vertical pile and the pipeline described in Section 7 and Section 8, respectivly. The seastate is still assumed to be stationary narrowbanded and wave

dominated. Further, the formulas for regular waves plus current are assumed to be valid for irregular waves plus current as well.

9.1 Burial

By employing Eqs. (68) and (66) and recalling that $\theta = \theta_m/\theta_{rms}$ Eq. (38) can be re-arranged to

$$B_d = Dc_1 \frac{U_{rms} w_c}{U_{rms} w_c + U_c} \left(\theta_{rms} w_c^{2-d} KC_{rms} w_c\right)^{c_2} \tag{84}$$

where $U_{rms} w_c = U_m$. Since KC_{rms}, θ_{rms} and U_{rms} are defined by the seastate alone, regardless of any current, it is convenient to introduce $\hat{B}_d$ given as

$$\hat{B}_d(w_c) = \frac{B_d/D}{c_1(\theta_{rms} KC_{rms})_2^c} = \frac{w_c}{w_c + U_c/U_{rms}} w_c^{c_2(3-d)} \tag{85}$$

The expected burial depth caused by the 1/n'th largest waves is given from Eq. (62) if S is replaced by $\hat{B}_d$

$$E[\hat{B}_d(w_c)|w_c > w_{c1/n}] = n \int_{w_{c1/n}}^{\infty} \hat{B}_d(w_c) p(w_c) dw_c \tag{86}$$

where $p(w_c)$ is the probability density function which can be derived from $P(w_c)$ given in Eq. (54)

$$p(w_c) = \frac{dP(w_c)}{dw_c} = \left(\frac{1}{\sqrt{8}\alpha}\right)^{\beta} \beta w_c^{\beta-1} \exp\left[-\left(\frac{w_c}{\sqrt{8}\alpha}\right)^{\beta}\right] \quad \text{for} \quad w_c \geq 0 \tag{87}$$

The value of w_c which exceeded with a probability of 1/n is found by solving $1 - P(w_{c1/n}) = 1/n$

$$w_{c1/n} = \sqrt{8}\alpha \left(\ln n\right)^{1/\beta} \tag{88}$$

It can be noted that the expressions for $p(w_c)$ and $w_{c1/n}$ can be obtained by inserting $w_{cl} = 0$ in Eqs. (75) and (74), respectivly.

Myrhaug and Ong (2009) presented the expected burial depth $\hat{B}_d$ for linear random waves in combined waves and current where $U_{rms}/(U_{rms} + U_c)$ was in the range of 0.5 to 1 and with $n = (3, 10)$ in their Fig. 3. In terms of U_{cwrms} this corresponds to the range of 0 to 0.5 which is a bit beyond wave dominated region. Further, Eq. (38) is strictly valid for $U_{rms}/(U_{rms} + U_c) \geq 0.8$. In order to study the influence of A_{rms}/z_0 they calculated the burial depth for each case of the coefficient d given in Eqs. (8)-(10).

Fig. 26 illustrates the expected equilibrium burial depth $\hat{B}_d$ from 3D, 2D and linear waves for $KC_{rms} = (25, 50)$, $d = 1$, $n = 10$ and $U_{rms}/(U_{rms} + U_c)$ in the same range as Myrhaug and Ong (2009). The seastate is given by $H_s = 3$m, $h = 10$m and the diameter is $D = 0.5$m. Accordingly, based on the Ursell criterion, the upper limit in KC_{rms} is 23.2. As expected, it appears that the burial depth for linear waves is equal to the results by Myrhaug and Ong (2009). By investigating Eq. (85) it appears that θ_{rms} and KC_{rms} must be given in order to determine the dimensional burial depth B_d. For linear waves, this involves that the expected value of $\hat{B}_d$ is independent of θ_{rms} and KC_{rms}, but as a consequence the Forristall effect in

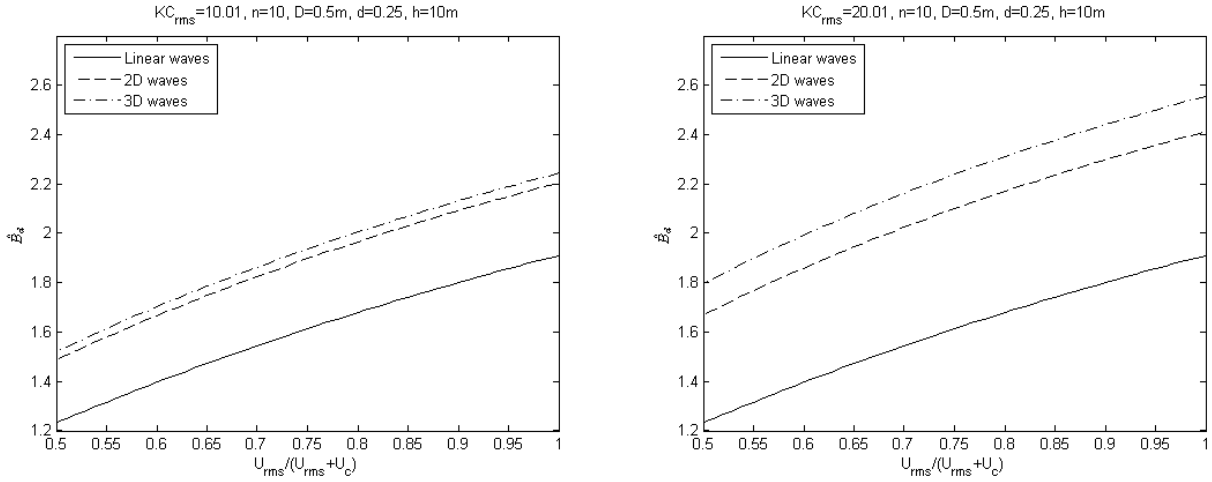

(a) $KC_{rms} = 10$ (b) $KC_{rms} = 20$

Figure 26: Expected burial depth for linear, 2D and 3D random waves versus $U_{rms}/(U_{rms}+U_c)$

Section 6.3.2, the expected value of $\hat{B}_d$ for 2D and 3D waves dependent on KC_{rms}. Figs. 26 and 40 (see Appendix B) clearly illustrate this. Accordingly, the expected value of $\hat{B}_d$ for linear waves is independent of the diameter.

Fig 27 illustrates the ratios of burial depth as a function of KC_{rms} for $U_{rms}/(U_{rms}+U_c) = 0.8$. It appears that 2D and 3D waves induce more scour than linear waves for all KC_{rms}. The reason for the increase in R_1 (2D waves) and R_1 (3D waves) for the low range values of KC_{rms} is due to high burial response from 2D and 3D. For $KC_{rms} \gtrsim 15$ the burial for 3D waves is larger than for 2D waves whereas for lower KC_{rms} the 2D waves will cause larger burial depth.

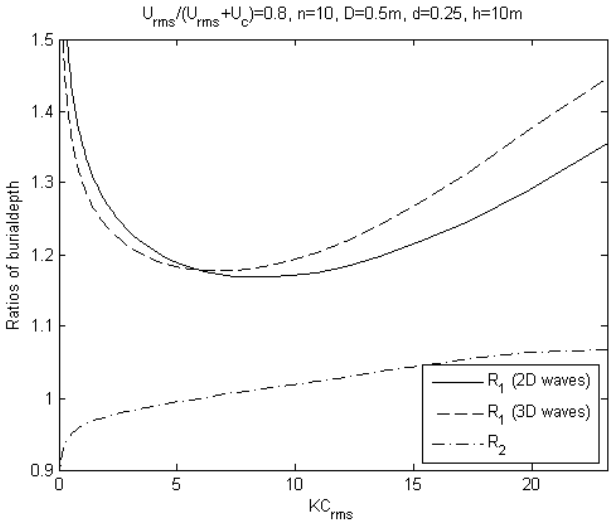

Figure 27: Ratios of burial depth versus KC_{rms}.

9.2 Scour

By employing Eq. (68), Eq. (40) can be re-arranged to

$$\hat{L} = \frac{L}{D} = p_1 KC_{rms}^{p_2} w_c^{p_2} \tag{89}$$

The expected scour hole length caused by the 1/n'th largest waves is given from Eq. (62) by replacing S with $\hat{L}$

$$E[\hat{L}(w_c)|w_c > w_{c1/n}] = n \int_{w_{c1/n}}^{\infty} \hat{L}(w_c) p(w_c) dw_c \tag{90}$$

where $p(w_c)$ and $w_{c1/n}$ are given in Eqs. (87) and (88), respectivly.
Myrhaug and Ong (2009) presented the expected total length of the scour hole for linear and Stokes second order random waves with $n = (3, 10)$ and cylinder aspect ratio $a_r = 4$ in their Fig. 4. Fig. 28 illustrates the expected total length of the scour hole around a short cylinder where $n = 10$ versus KC_{rms}. The seastate is given by $H_s = 3$m, $h = 10$m and the diameter of the cylinder is $D = 0.5$m. Accordingly, based on the Ursell criterion, the upper limit in KC_{rms} is 23.2. As expected, it appears that the total scour hole length for linear waves is equal to the results by Myrhaug and Ong (2009). It should be noted that the result from linear waves is valid for any diameter corresponding to the given validity range in KC of Eq. (40). However, due to the Forristall effect in Section 6.3.2, the results from 2D and 3D waves are only valid for $D = 0.5$m.

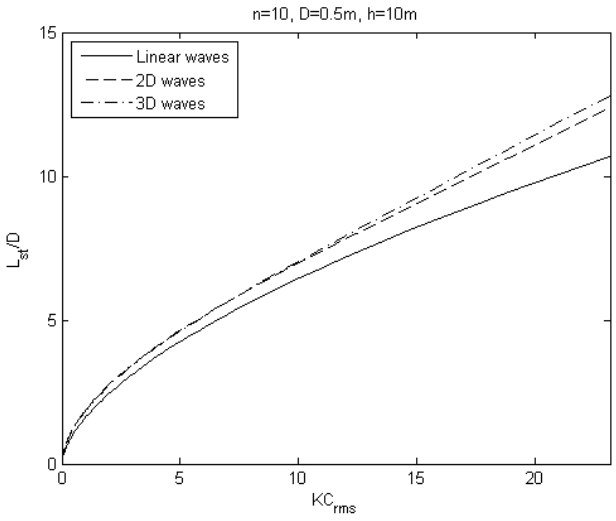

Figure 28: Expected total length of scour hole versus KC_{rms}.

Fig. 29 illustrates the ratios of scour hole length as a function of KC_{rms} corresponding to Fig. 28. It appears that 2D and 3D waves induce more scour than linear waves for all KC_{rms}. The reason for the sudden increase in R_1 (2D waves) and R_1 (3D waves) at the low range values of KC_{rms} is due to low scour respons from linear waves. For $KC_{rms} \gtrsim 6$ the 3D waves induce more scour than 2D waves whereas for lower KC_{rms} the 2D waves will generate more scour.

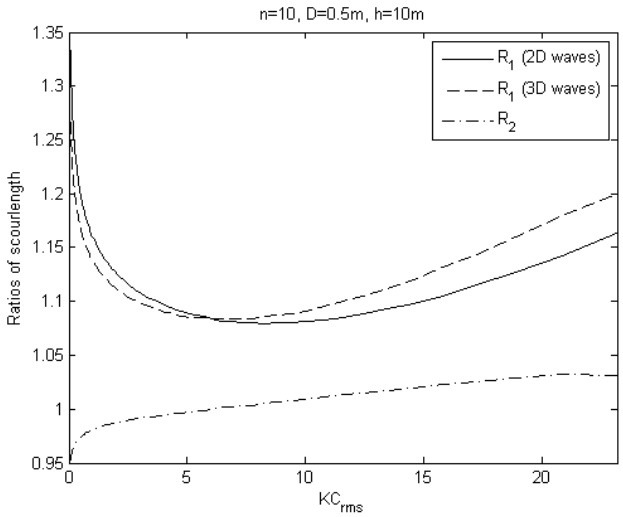

Figure 29: Ratios of total length of scour hole versus KC_{rms}.

9.3 Example of calculation

The following example of calculation of the burial depth and scour hole geometry around a short cylinder is presented in order to demonstrate the application of the method and based on the same flow condition as the vertical pile described in Table 1. The results for 3D, 2D and linear random waves alone are given in Table 4 for a cylinder diameter $D = 0.5$m and aspect ratio $a_r = 4$. The burial depth is also given for $U_{rms}/(U_{rms} + U_c) = 0.804$.

By rearranging Eq. (85) the burial depth can be written as $B_d = Dc_1(\theta_{rms}KC_{rms})^{c_2}\hat{B}_d$, where $\hat{B}_d$ is presented in Fig. 26 for 3D, 2D and linear waves plus current. The coefficients (c_1, c_2) are given in Eq. (39). From Table 4 it appears that the current will reduce the burial depth, which is consistent with the features of $\hat{B}_d$ in Fig. 26. Further, the 3D waves will cause the largest burial depth followed by 2D and linear waves.

By rearranging Eq. (90) the totale length of the scour hole can be written as $L_{st} = Dp_1(KC_{rms}w_c)^{p_2} = D\hat{L}_{st}$ where $\hat{L}_{st}$ is presented in Fig. 28. The coefficients $p_1 = 0.75a_r^{0.3} = 1.14$ as $a_r = 4$ and $p_2 = 0.6$. It should be noted that, similar to the case of burial, the 3D waves will cause the largest scour hole, followed by 2D and linear waves. This is caused by smaller set-down effects for 3D waves in finite water depth compared to 2D waves.

10 Conclusion

For all the various cases of scour and burial it appears that the ratios R_1 (3D waves), R_1 (2D waves) and R_2 in Figs. 20, 21, 22, 23, 25, 27 and 29 display similar features. Similar tendencies are also detected in the examples of calculation. Overall, it can be noted that the nonlinear 2D and 3D waves will cause more scour and burial than linear waves although the ratios varies with the presence of current and the KC-number.

Moreover, it appears that scour from 2D waves is larger than the 3D counterpart for the lowest values of KC_{rms} whereas the scour depth from 3D waves will dominate for higher KC_{rms}. Recalling that KC_{rms} will increase as the water depth decreases this behaviour in

Table 4: Short cylinder with $D = 0.5$m and flow conditions given in Table 1

KC_{rms} Eq. (51)	12.98
Burial:	
Waves alone:	
$B_{d,lin}$ (m)	0.348
$B_{d,nonlin,2D}$ (m)	0.409
$B_{d,nonlin,3D}$ (m)	0.422
Waves plus current:	
$B_{d,lin}$ (m)	0.307
$B_{d,nonlin,2D}$ (m)	0.366
$B_{d,nonlin,3D}$ (m)	0.378
Total length of scour hole:	
Waves alone:	
$L_{st,lin}$ (m)	3.766
$L_{st,nonlin,2D}$ (m)	4.105
$L_{st,nonlin,3D}$ (m)	4.173

$R2$ is due to the larger wave setdown effects for 2D waves than for 3D waves in shallow water. However, in deep water the difference frequency effects disappears and the 2D waves will dominate due higher sum frequency effects compared to 3D waves.

Even though the stochastic method presented in this report is simple, it may be usefull as an engineering tool for estimating the scour depth beneath 2D and 3D nonlinear random waves plus current for vertical piles, pipelines and short cylinders. More experimental data is necessary in order to discuss the validity of this method.

Glossary

Symbol	Description
α	Shear stress amplification factor
τ	Shear stress
τ_∞	Undisturbed shear stress
S	Equilibrium scour depth
S_t	Instantanious scour depth
t	Time
T	Time scale of scour
θ	Shields parameter
ρ	Density of water
g	Acceleration of gravity
ρ_s	Sediment density
s	Ratio between ρ_s and ρ
d_{50}	Median grain diameter
θ_{cr}	Critical value of Shields parameter
f_w	Friction factor
U_m	Maximum horizontal fluid velocity at the seabed
A	Orbital displacement of water particles at the seabed
z_0	Bed roughness
(c, d)	Coefficients for calculating the friction factor
H	Linear wave height
h	Water depth
k	Wave number
ω	Angular wave frequency
KC	Keulegan-Carpenter number
D	Charateristic diameter
T	Wave period
(C, q, r)	Coefficients for calculating pile scour
G	Gap between vertical piles
U_{rms}	Root-mean-square value of U_m
T_p	Peak periode of the wave spectrum
T_z	Mean zero crossing wave periode
KC_{SF}	KC based on T_p in experimental data from Sumer and Fredsøe (1996, 2001)
U_c	Current velocity
U_{cwrms}	Coefficient based on U_c and U_{rms}
U_{cw}	Coefficient based on U_c and U_m
S_{cur}	Scour depth for pipeline in current alone
F	Non-dimensional parameter utilized for pipeline scour

Symbol	Description
(a, b)	Coeffcients for calculating pipeline scour
B_d	Burial depth
L_c	Length of short cylinder
(c_1, c_2)	Coefficients for calculating burial
a_r	Aspect ratio
L	Representation of scour hole length
(p_1, p_2)	Coefficients for calculating scour hole geometry
L_{st}	Total length of scour hole
L_{sd}	Downstream length of scour hole
L_{su}	Upstream length of scour hole
W	Width of scour hole around short cylinder
η_c	Crest height
a	Amplitude of first harmonic wave component
ω_p	Peak frequency
k_p	Wave number corresponding to ω_p
w_c	Dimensionless crest height
a_{rms}	Root-mean-square value of crest height
$\hat{a}$	Dimensionless crest height
$\hat{U}_m$	Dimensionless maximum horizontal fluid velocity at the seabed
KC_{rms}	Root-mean-square value of the Keulegan-Carpenter number
$P(w_c)$	Cumulative distribution function
α_{2D}, β_{2D}	Dimensionless coefficients in Forristall distribution for long-crested waves
β_{3D}, β_{3D}	Dimensionless coefficients in Forristall distribution for short-crested waves
S_1	Wave steepness
U_R	Ursell number
T_1	Mean spectral periode
k_1	Wavenumber corresponding to T_1
H_S	Significant wave height
w_{c1}	Lower limit of w_c
w_{c2}	Upper limit of w_c
$w_{c1/n}$	Value of w_c exceeded with a probability of $1/n$
R_1(3D waves)	Ratio between 3D and linear waves
R_1(2D waves)	Ratio between 2D and linear waves
R_2	Ratio between 3D and 2D waves
θ_c	Dimensionless Shields parameter
θ_m	Maximum Shields parameter
θ_{rms}	Root-mean-square value of Shields parameter
A_{rms}	Root-mean-square value of the orbital displacement at the seabed
τ_c	Dimensionless seabed shear stress
$p(w_c)$	Probability density function
$H(x - x_0)$	Heaviside function

References

Catano-Lopera, Y. and Garcia, M. (2006). Burial of short cylinders induced by scour under combined waves and currents. *J. Waterway port, coastal and ocean engineering*, 132:439–449.

Catano-Lopera, Y. and Garcia, M. (2007). Geometry of scour hole around , and the influence of the angle of attack on the burial of finite length cylinders under combined flows. *Ocean Engineering*, 34:856–869.

Forristall, G. Z. (2000). Wave crest distributions: Observations and second-order theory. *Journal of Physical Oceanography*, 30(8):1931–1943.

Jensen, B., Sumer, B., Jensen, R., and Fredsøe, J. (1990). Flow around and forces on a pipeline near a scoured bed in steady current. *J. Offshore mechanics and artic engineering*, 12:206–213.

Myrhaug, D. (2006). *TMR4230 Oceanography.* NTNU Trondheim.

Myrhaug, D. and Holmedal, L. E. (2011). Bottom friction and erosion beneath long-crested and short-crested nonlinear random waves. Submitted for publication.

Myrhaug, D., Holmedal, L. E., Simmons, R. R., and MacIver, R. D. (2001). Bottom friction in random waves plus current. *Coastal Engineering*, 43:75–92.

Myrhaug, D. and Ong, M. C. (2009). Burial and scour of short cylinders under combined random and currents including effects of second order wave asymmetry. *Coastal Engineering*, 56:73–81.

Myrhaug, D., Ong, M. C., Føien, H., Gjengedal, C., and Leira, B. J. (2009). Scour below pipelines and around verticla piles due to second order random waves plus current. *Ocean Engineering*, 36:605–616.

Myrhaug, D. and Rue, H. (2003). Scour below pipieline and around vertical piles in random waves. *Coastal Engineering*, 48:227–242.

Myrhaug, D. and Rue, H. (2005). Scour around group of slender vertical piles in random waves. *Applied Ocean Research*, 27:56–63.

Sarpkaya, T. (1986). Force on a circular cylinder in viscous oscillatory flow at low keulegan-carpenter numbers. *J. Fluid Mechanics*, 165:61–71.

Sumer, B. and Fredsøe, J. (1990). Scour below pipelines in waves. *J. Waterway port, coastal and ocean engineering*, 116:307–323.

Sumer, B. M., Christiansen, N., and Fredsøe, J. (1993). Influence of cross section on wave scour around piles. *J. Waterway, Port, Coastal and Ocean Engineering*, 119:477–495.

Sumer, B. M., Christiansen, N., and Fredsøe, J. (1997). Horseshoe vortex and vortex shedding around a vertical wall-mounted cylinder exposed to waves. *J. Fluid Mechanics*, 332:41–70.

Sumer, B. M. and Fredsøe, J. (1996). Scour below pipelines in combined waves and current. In *Proceedings of the 15th international conference on OMAE*, volume 15.

Sumer, B. M. and Fredsøe, J. (1998). Wave scour around group of vertical piles. *J. Waterway port, coastal and ocean engineering*, 124:248–256.

Sumer, B. M. and Fredsøe, J. (2001). Scour around a pile in combined waves and current. *J. Hydraulic Engineering*, 127:403–411.

Sumer, B. M. and Fredsøe, J. (2002). *The Mechanics of Scour in the Marine Environment.* World Scientific Publishing Co. Pte. Ltd.

Sumer, B. M., Fredsøe, J., and Christiansen, N. (1992). Time scale of scour around a vertical pile. In *Proc. second Int. Offshore and Polar Eng. Conf.*

Wist, H. T. (2003). *Statistical properties of successive ocean wave parameters.* PhD thesis, NTNU Trondheim.

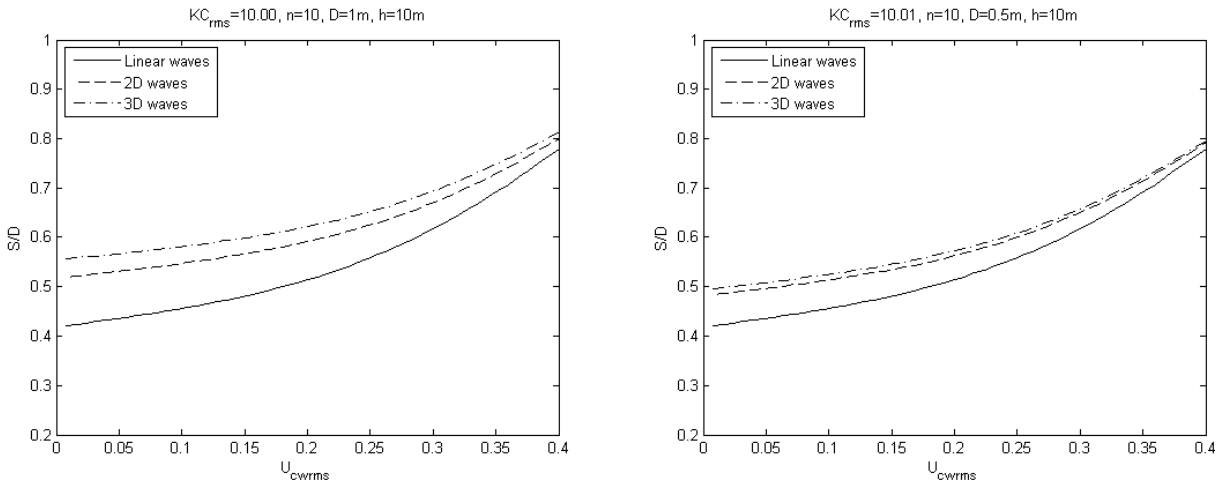

(a) $D = 1$m (b) $D = 0.5$m

Figure 30: Nondimensional scour depth for circular pile versus U_{cwrms}

A Vertical Piles

This appendix is a gathering of the results of the expected equilibrium scour depth for the various pile arrangements presented in Section 7, both single and multiple piles. The results are based on $H_s = 3$m, $h = 10$m and the diameter is specified in each case.

A.1 Circular cross section

Fig. 30 illustrates the nondimensional scour depth S/D versus U_{cwrms} exemplified for $KC_{rms} = 10$, $n = 10$ and two different diameters. As mentioned, the nondimensional scour depth for linear waves is equal in the two cases, whereas this is not the case for 2D and 3D waves due to the Forristall effect in Section 6.3.2. It appears that $D = 0.5$m will cause less nondimensional scour than $D = 1$m for both 2D and 3D waves. Fig. 31 illustrates the ratios between the expected equilibrium scour depths presented in Fig. 19. For $KC_{rms} = 2.67$, both R_1 (3D waves) and R_1 (2D waves) are higher than for $KC_{rms} = 5.33$ for any given U_{cwrms}. Further, R_2 is lowest when $KC_{rms} = 2.67$. The ratios are highest for zero current velocity and when the current velocity is increased it appears that the ratios decrease.

Fig. 32 illustrates the expected equilibrium scour depth around a circular pile versus KC_{rms} for $U_{cwrms} = 0$ and 0.4. Fig. 33 illustrates the ratios of expected equilibrium scour depth around a circular pile versus KC_{rms} for $U_{cwrms} = 0$ and 0.4 corresponding to Fig 32.

A.2 Square cross section

Fig. 34 illustrates the expected equilibrium scour depth for the 45° and 90° square pile versus KC_{rms} based on the ratios in Fig. 21. It appears that the 45° square pile will experience the highest amount of scour regardless of KC_{rms}. Fig. 7 displays the same characteristics.

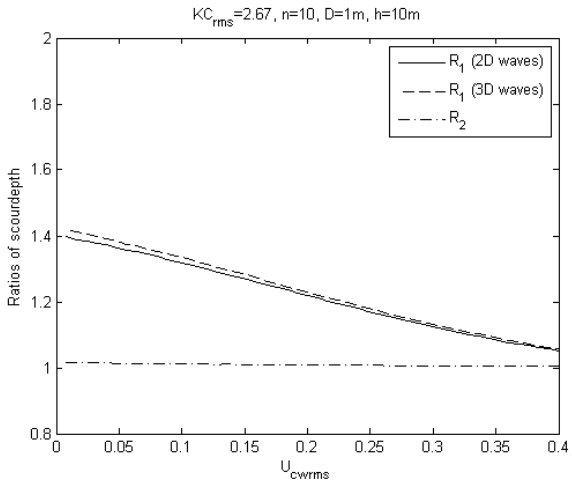

(a) Ratios for $KC_{rms} = 2.67$

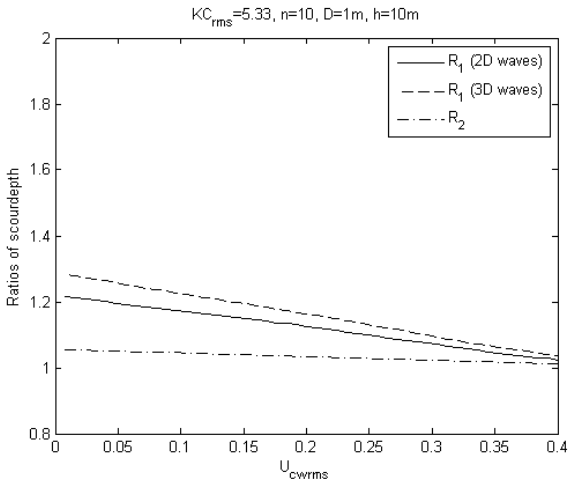

(b) Ratios for $KC_{rms} = 5.33$

Figure 31: Ratios of scour depth around circular cylinder versus U_{cwrms}

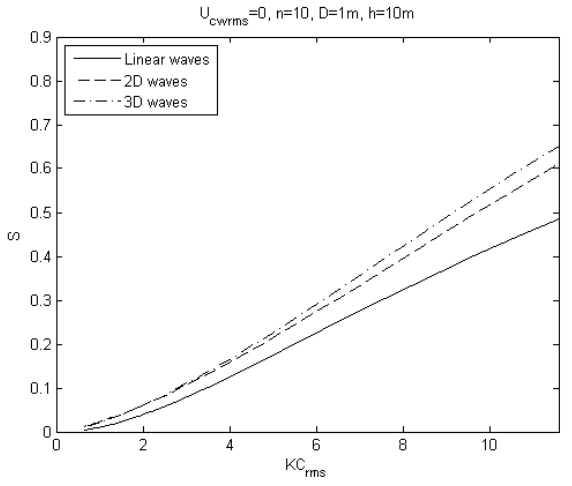

(a) $U_{cwrms} = 0.0$

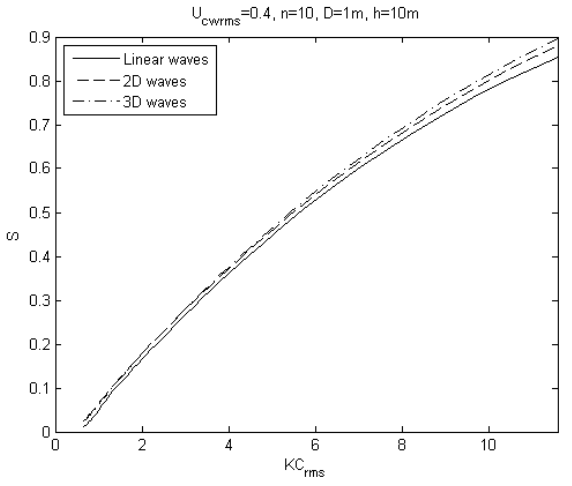

(b) $U_{cwrms} = 0.4$

Figure 32: Scour depth for circular pile versus KC_{cwrms}

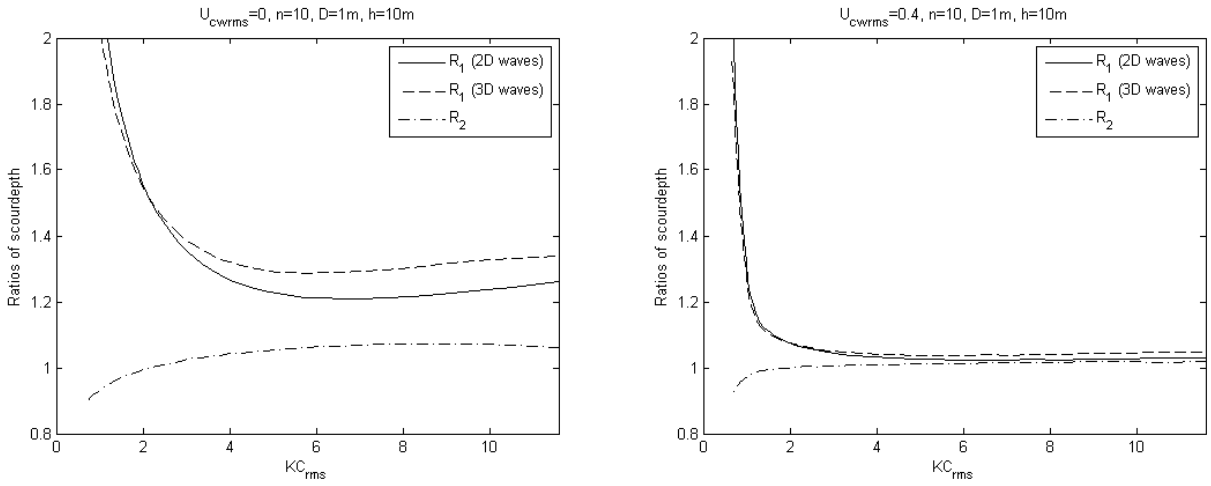

(a) $U_{cwrms} = 0.0$ (b) $U_{cwrms} = 0.4$

Figure 33: Ratios of scour depth for circular pile versus KC_{cwrms}

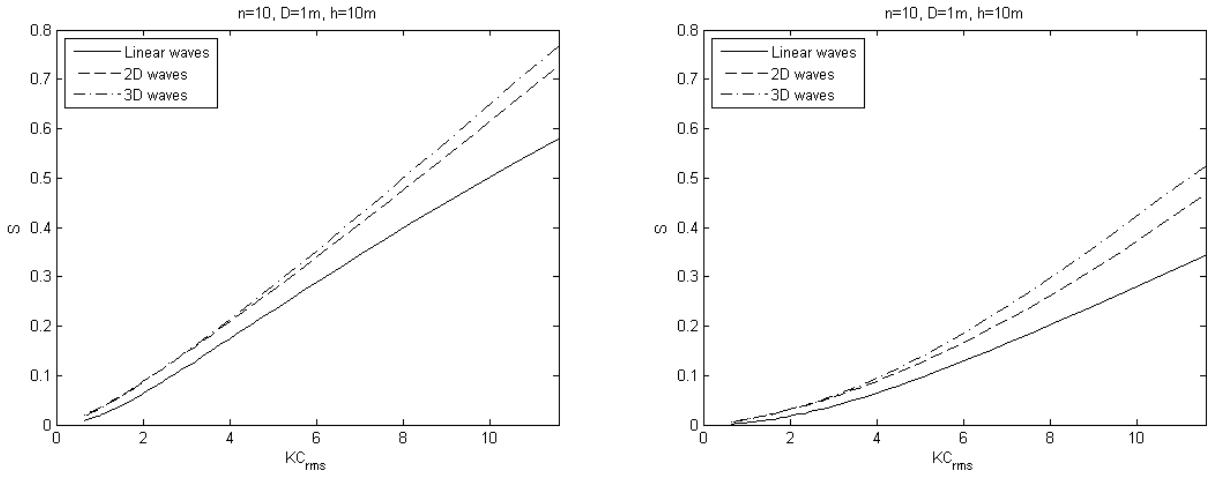

(a) 45° (b) 90°

Figure 34: Scour depth for square pile versus KC_{cwrms}

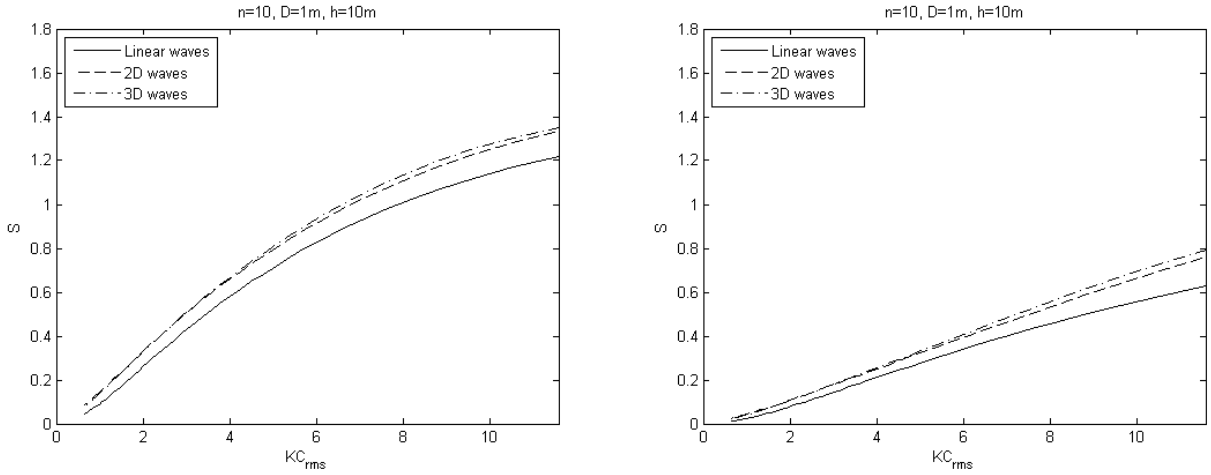

(a) Side-by-side (b) 45° staggered

Figure 35: Scour depth for two-pile groups versus KC_{rms}

A.3 Group arrangements

Figs. 35 and 36 illustrate the maximum expected equilibrium scour depth for the side-by-side, 45° staggered and 4×4 group arrangements. It appears that for the maximum values of KC_{rms} the 4×4 arrangement will be subject to the largest amount of scour whereas the 45° staggered arrangement will cause the smallest amount. For mid-range values of KC_{rms} the side-by-side arrangement will experience the most scour. Fig. 11 displays the same characteristics.

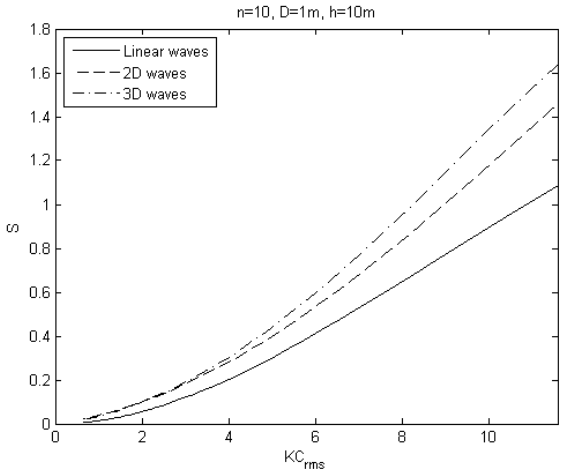

Figure 36: Scour depth around 4×4 group of piles versus KC_{rms}.

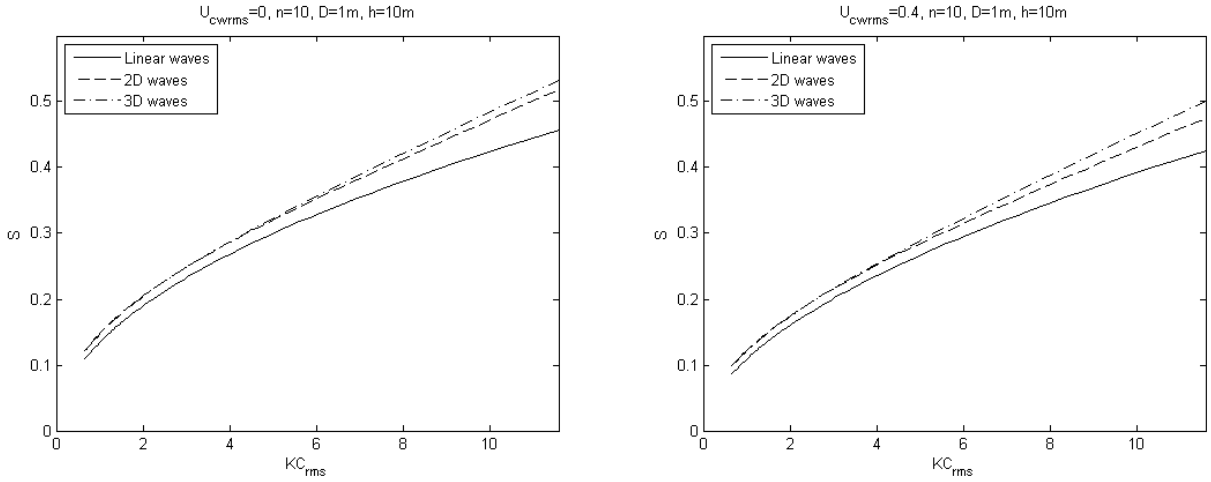

(a) $U_{cwrms} = 0.0$ (b) $U_{cwrms} = 0.4$

Figure 37: Scour depth for pipeline versus KC_{cwrms}

B Pipelines and short cylinders

This appendix is a gathering of the supplementary results of the expected equilibrium scour depth for pipelines and short cylinders presented in Section 8 and 9. The results are based on $H_s = 3$m, $h = 10$m and the diameter is specified in each case.

B.1 Pipelines

Fig. 37 illustrates the expected equilibrium scour depth around a pipeline versus KC_{rms} for $U_{cwrms} = 0$ and 0.4. Fig. 38 illustrates the ratios of expected equilibrium scour depth around a pipeline versus KC_{rms} for $U_{cwrms} = 0$ and 0.4 where the former corresponds to waves alone.

Fig 39 illustrates the ratios between the expected equilibrium scour depths presented in Fig. 24. For both cases of KC_{rms} it appears that in the lower half of the current velocity range there is an increase in R_1 (2D waves) and R_1 (3D waves) after which the ratios decrease. R_2 appears to increase at a constant rate with U_{cwrms}. The variations with KC_{rms} in this range are small but it seems that all the ratios have increased for $KC_{rms} = 6.67$ where the largest growth in R_1 (3D waves) is found.

B.2 Burial of short cylinder

Fig. 40 illustrates the burial depth for $U_{rms}/(U_{rms} + U_c) = 0.8$ and 1 where the latter corresponds to waves alone.

Fig. 41 illustrates the ratios of expected burial depth corresponding to Fig. 26. The reason why R_1 (2D waves) and R_1 (3D waves) are higher for $KC_{rms} = 20$ is due to larger burial depths for 2D and 3D waves as the linear burial depth is constant.

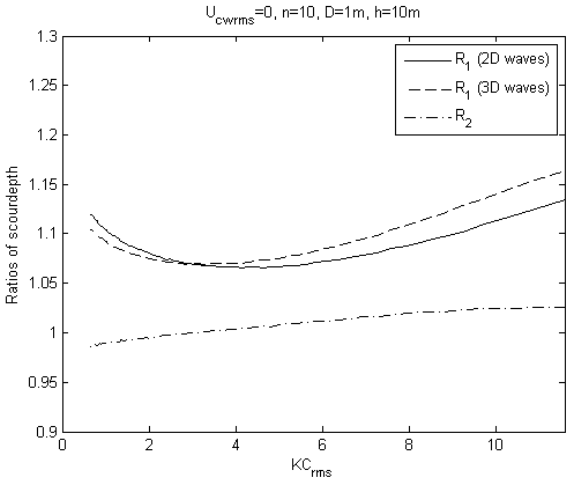

(a) $U_{cwrms} = 0.0$

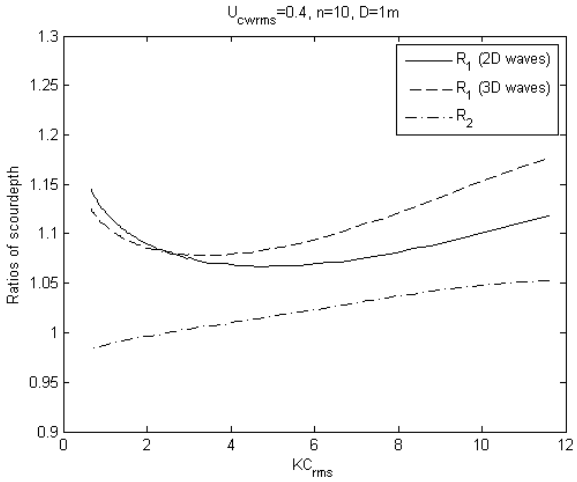

(b) $U_{cwrms} = 0.4$

Figure 38: Ratios of scour depth for pipeline versus KC_{cwrms}

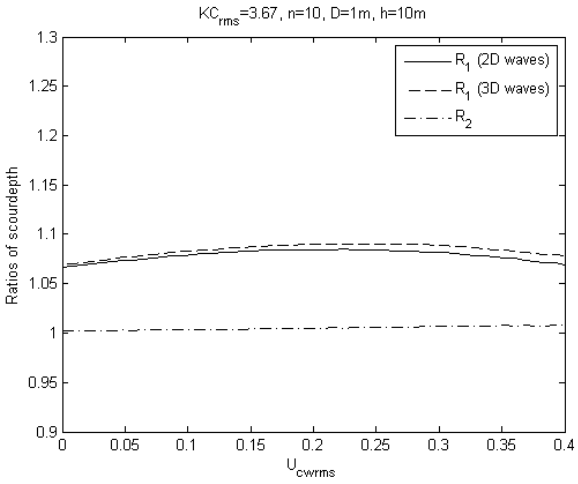

(a) Ratios for $KC_{rms} = 3.67$

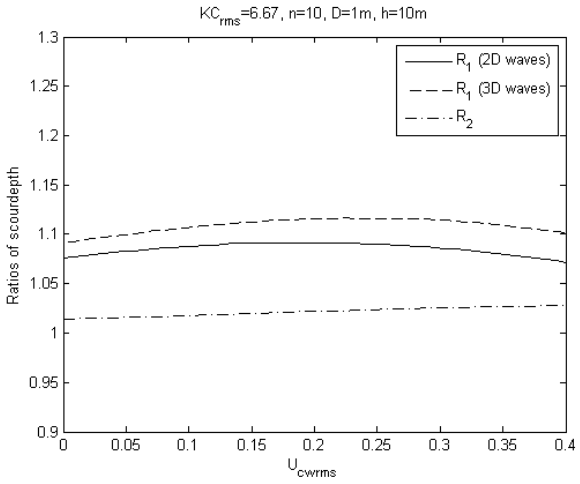

(b) Ratios for $KC_{rms} = 6.67$

Figure 39: Ratios of scour depth around a pipeline versus KC_{rms}

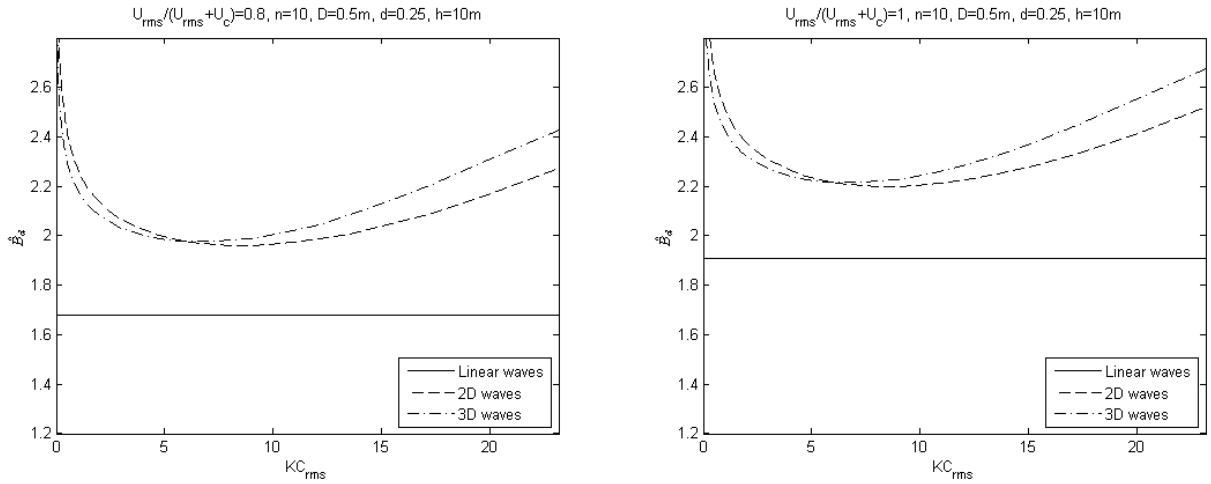

(a) $U_{rms}/(U_{rms}+U_c)=0.8$ (b) $U_{rms}/(U_{rms}+U_c)=1$

Figure 40: Burial depth for short cylinder versus KC_{cwrms}

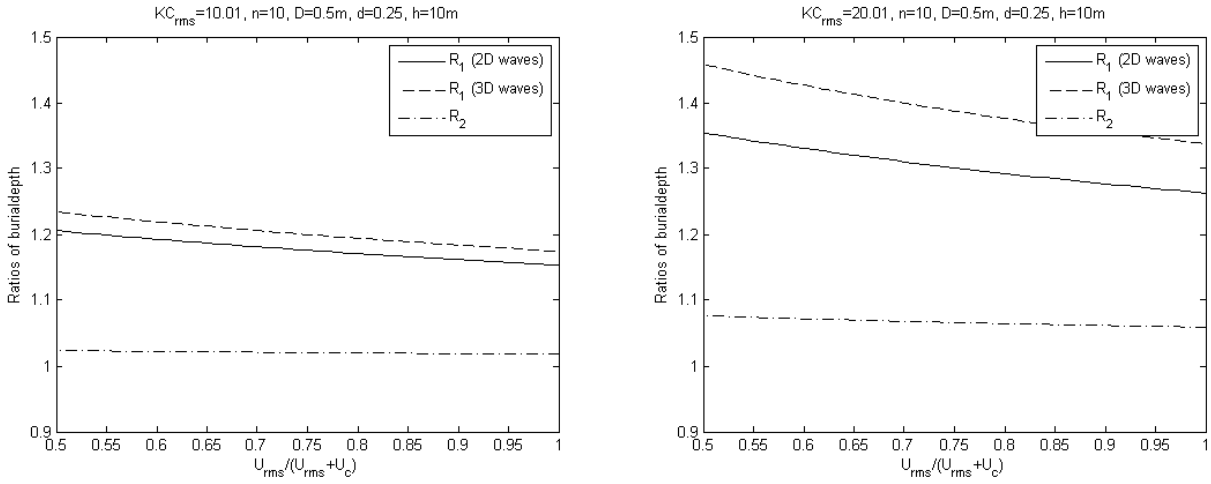

(a) $KC_{rms}=10$ (b) $KC_{rms}=25$

Figure 41: Ratios of expected burial depth for linear, 2D and 3D random waves versus $U_{rms}/(U_{rms}+U_c)$